THE ANALYSIS OF THE REFERENCE SHAFT UNDER TORQUE MEASUREMENT UNIT FOR TURBOSHAFT ENGINES

by
KEREM KILIÇ

Submitted to the Graduate School of Engineering and Natural Sciences
in partial fulfilment of
the requirements for the degree of Master of Science

Sabancı University
December 2020

THE ANALYSIS OF THE REFERENCE SHAFT UNDER TORQUE MEASUREMENT UNIT FOR TURBOSHAFT ENGINES

Approved by:

Approval Date: December 25, 2020

ABSTRACT

THE ANALYSIS OF THE REFERENCE SHAFT UNDER TORQUE MEASUREMENT UNIT FOR TURBOSHAFT ENGINES

KEREM KILIC

ENERGY TECHNOLOGIES and MANAGEMENT M.Sc THESIS, DECEMBER 2020

Thesis Supervisor: Asst. Prof. BEKIR BEDIZ

Keywords: Torque Measurement, Angular Twist Method, Reference Shaft, Torquemeter, Turboshaft Engine

Gas turbine engines have become a dominating and convincing power source in aviation; for instance, turboshaft gas turbine engines are widespread propulsion systems for helicopters. In turboshaft engines, produced power is transmitted to the helicopter rotor group via a power output shaft. The level of power extraction depends on the transmitted torque and rotational speed of the power output shaft. The need to measure the torque from a rotating shaft leads to the development of various torque measurement units. The commonly used torque measurement unit (TMU) of compact turboshaft engines makes use of an angular twist method. The angular twist method is a multidisciplinary approach with a strong base in mechanics, electronics, and control. In this thesis, a comparison of TMU of various turboshaft engines, which use the angular twist method, is done concerning mechanical discipline. The new generic conceptual design of the reference shaft is done under TMU to be used for different turboshaft engines with minor modifications. The reference shaft is analyzed in terms of strength and vibration criteria. Static structural analysis is done to examine the mechanical integrity of the reference shaft. X-ray diffraction method is used to measure the residual stresses on the reference shaft. Modal analysis is done for vibration characteristics, and it is validated via the impact hammer test. Finally, the measurement accuracy of the TMU and the need for calibration are discussed in future work.

ÖZET

TURBOŞAFT MOTORLARI İÇİN TORK ÖLÇÜM ÜNİTESİ ALTINDA REFERANS ŞAFT ANALİZİ

KEREM KILIÇ

ENERJİ TEKNOLOJİLERİ VE YÖNETİMİ YÜKSEK LİSANS TEZİ, ARALIK 2020

Tez Danışmanı: Dr. Öğr. Üyesi BEKİR BEDİZ

Anahtar Kelimeler: Tork Ölçümü, Açısal Burulma Yöntemi, Referans Şaft, Torkmetre, Turboşaft Motor

Gaz türbinli motorlar havacılıkta hakim ve etkili güç kaynağı haline gelmiştir. Örnek olarak, turboşaft gaz türbinli motorları helikopterler için yaygın tahrik sistemleridir. Turboşaft motorlarda üretilen güç, güç çıkış şaftı vasıtasıyla helikopterlerin rotor grubuna iletilir. Güç seviyesi, iletilen torka ve güç çıkış şaftının dönme hızına bağlıdır. Dönen bir şafttan tork ölçme ihtiyacı, çeşitli tork ölçüm sistemlerinin geliştirilmesine öncülük etmiştir. Kompakt turboşaft motorlarda yaygın olarak kullanılan tork ölçüm sistemleri (TÖS) açısal burulma yönteminden faydalanır. Açısal burulma yöntemi mekanik, elektronik ve kontrol alanlarında güçlü bir temeli olan çok disiplinli bir yaklaşımdır. Bu tezde çeşitli turboşaft motorların açısal burulma yönteminden faydalanan TÖS'lerinin karşılaştırılması mekanik disiplin açısından yapılmıştır. Yeni bir jenerik referans şaftın kavramsal tasarımı TÖS altında yapılmıştır, bu referans şaft küçük modifikasyonlarla farklı turboşaft motorları için kullanılabilir. Referans şaft, mukavemet ve titreşim kriterleri açısından analiz edilmiştir. Referans şaftın mekanik bütünlüğünü incelemek için statik yapısal analiz yapılmıştır. X ışını kırınımı yöntemi, referans şaft üzerindeki kalıntı gerilmeleri ölçmek için kullanılmıştır. Referan şaftın titreşim karakteristiği için modal analiz yapılmış ve çekiç testi ile doğrulanmıştır. Son olarak gelecek çalışmalar kısmında, TÖS'lerin ölçüm hassasiyetleri ve kalibrasyon ihtiyacı tartışılmaktadır.

ACKNOWLEDGEMENTS

I would like to express my special thanks to my advisor Asst. Prof. Bekir Bediz. Through his actions, he has shown me how research should be done and how an academician should be. I would also like to thank my jury members Asst. Prof. Eralp Demir, Asst. Prof. Recep Önler and all the members of the Faculty of Engineering and Natural Sciences of Sabanci University who kindly shared the knowledge and experience with me.

I also would like to express my special thanks to my company, TEI for all of the opportunities and support that have been provided for me. My colleagues also deserve to be acknowledged, I am grateful for all their contributions to this work. I would like to express my gratitude to my manager Dr. Serdar Aksoy. It is only with his support, guidance, and encouragement that I have been able to complete this process. It has been a privilege to work for TEI.

I would also like to thank all my close friends who support me, encourage me, helped me, and made the journey pleasurable and rewarding. I would like to especially thank Mahmut Furkan Tüfekçi for his support.

I would like to express my sincere gratitude to my parents, my sister, and my brother for their endless blessing, love, and selfless support over the years. I am grateful for everything they have done for me. I also would like to express my special thanks to my wife for walking through the journey together with me, sharing the new horizon, and for her endless love.

Lastly and mostly, I express my sincere gratitude to Allah The Almighty for all the blessings and hardships, to whom all praise is. Alhamdulillah!

Surely with hardship comes ease

TABLE OF CONTENTS

LIST OF TABLES

LIST OF FIGURES

LIST OF ABBREVIATIONS

CAD: Computer-Aided Design

EASA: European Union Aviation Safety Agency

ECU: Engine Control Unit

FADEC: Full Authority Digital Engine Control

FEA: Finite Element Analysis

FOS: Factor of Safety

FRF: Frequency Response Function

HAZ: Heat Affected Zone

HCF: High Cycle Fatigue

LCF: Low Cycle Fatigue

TMU: Torque Measurement Unit

XRD: X-ray Diffraction

1. INTRODUCTION

The gas turbine engine has become the most widespread and effective method of aircraft propulsion systems after it became the dominating power source in aviation after the 1960s. The gas turbine engine can be categorized as a turbojet, turbofan, turboprop or turboshaft according to their task and design characteristics (Hünecke, 1997).

Today, gas turbine engines continue to be one of the most critical aviation technological achievements due to the precisely manufactured components and high-temperature resistant materials. An essential gas turbine includes two main rotating parts, a compressor and a turbine connected through a shaft; and a combustor (combustion chamber) (see Figure 1). The gas turbine operates on the Brayton cycle principle, where the ideal gas turbine is subjected to three thermodynamic processes: isentropic compression, isobaric combustion, and isentropic expansion. However, in practice, energy is lost to heat and pressure change because of friction and turbulence (Hünecke, 1997).

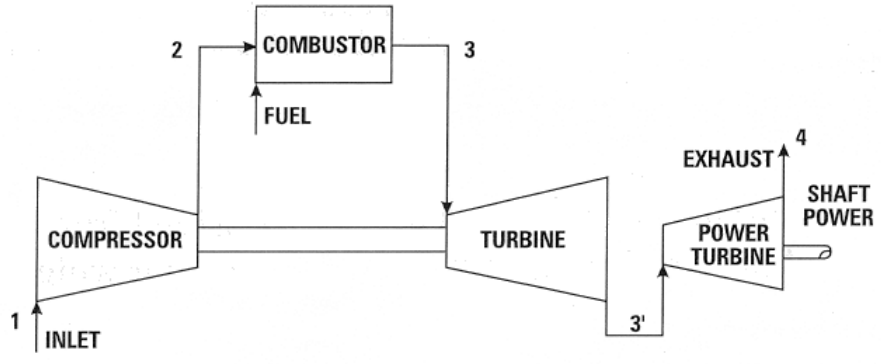

Figure 1. Mechanical arrangement of a gas turbine engine

Air is drawn from the atmosphere at the inlet during process one, as shown in Figure 1. Then, it is compressed by a compressor that increases air temperature, pressure, and

acceleration. During process 2, compressed air passes into the combustor, where the burning of injected fuel heats it. The resulting expansion of air causes a rise in pressure and temperature, so in the process three expanded and energy gained gas flows into a turbine. Finally, the gas transforms some of its energy and momentum to drive the turbine by passing through it, thereby supplying power to the compressor for operation. The processes until the turbine are generally standard in most gas turbine engines; the section includes compressor, combustor, and the turbine is usually called a core engine. However, an easy categorization between the forms of gas turbine engines is made according to the exhaust gas utilization after the turbine (Rolls-Royce, 1996).

If the exhaust gas is directly used to generate propulsive force, the engine is termed turbojet, which generally powers fighter jets. The engine is termed as a turbofan if the energy of exhaust gas after turbine partially used for propulsive force similar to turbojet; but also partially used to drive a separate turbine by passing through it, which supplies power for a fan at the inlet of the engine. The fan leads to a mass airflow that bypasses the basic engine, and it provides a propulsive force for turbofan engines. They are generally used in commercial airplanes.

If most of the energy of exhaust gas and its momentum is extracted by an additional separate power turbine by passing through it during process 3` as illustrated in Figure 1, the engine is called either turboprop or turboshaft depending on the use of shaft power that is converted from power turbine. If this shaft power is consumed to drive a propeller, then the engine is called a turboprop that is commonly used by fixed-wing aircraft. If the shaft power is transmitted directly to the drive train in the platform, the engine is termed as turboshaft, which is generally used to power up rotary-wing aircrafts such as helicopters. However, turboshaft engines can also be used for different power applications such as powering an automotive, a battle tank, or a ship (Hünecke, 1997) and (Rolls-Royce, 1996).

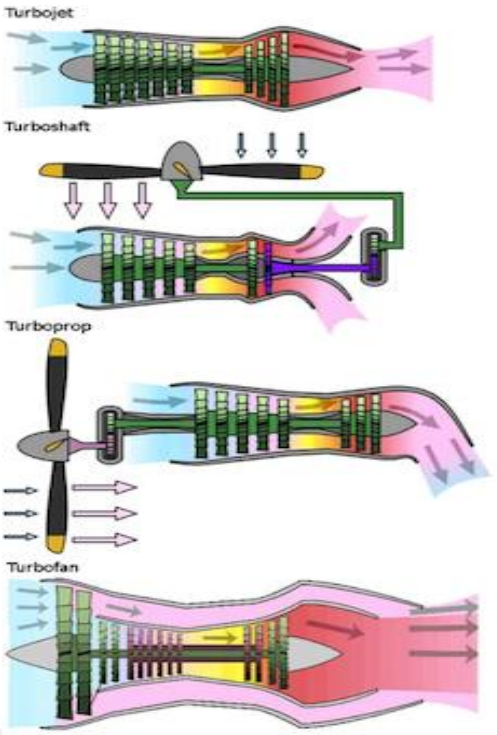

Figure 2. Types of Gas Turbine Engines *(Hünecke, 1997)*

In this thesis, the torque measurement units (TMU) in different benchmark turboshaft engines are compared in terms of the mechanical design aspect. The reference shaft's conceptual design and analysis as a subpart of a torque measurement unit for a turboshaft engine are elaborated.

1.1. **Torque measurement unit in Turboshaft Engine**

In a turboshaft engine, produced power is transmitted to the helicopter rotor group through an output power shaft. The power extraction variation from the power output shaft under different engine conditions depends on the transmitted torque and the power output shaft's rotational speed. Equation (1) shows that the shaft power (P) in Watt (W) is equal to transmitted torque (T) in Newton-meter (Nm) times shafts angular velocity (ω) in rad/sec. Torque is a vectorial quantity and causes rotational motion (NASA G. R., 2015)**.**

$$P\ [W] = T\ [Nm].\omega\ [rad/sec] \quad (1)$$

Besides, Eq. (2) indicates that torque is proportional to the moment of inertia and angular

acceleration of the shaft. Torque is equal to the shaft's moment of inertia (I) times the shaft's angular acceleration, which is the second derivative of shaft's angular displacement (θ) with respect to time (t) (Doebelin, 1966).

$$T = I\frac{d^2\theta}{dt^2} \tag{2}$$

The shaft rotational speed and transmitted torque measurements are critical since those two parameters dictate the turboshaft engine's performance, control, and safety. The measured rotational speed can be used as the primary control parameter for stable operation, and it is used to check engine performance characteristics. However, a helicopter pilot requires monitoring torque because only considering the shaft's speed is not enough to determine whether the engine's extracted power is within the desired range. Therefore, there are torque indicators in the platform for monitoring the measured torque value supplied by the engine. Additionally, in two turboshaft engine applications, the engine controller unit should match both engines' transmitted torque values to protect the helicopter's drive train and sustain its life requirement. (US Patent No. 3114240, 1963) (Chang & Kukel, 1973).

The need for measuring torque from a rotating shaft necessitates the development of various torque measurement techniques and equipment. The transmitted torque on the driving output shaft leads to angular deflection of the shaft, resulting in shear stress and strain. Although there are different measurement methods, a technique based on either angular twist or strain is usually selected based on the torque measurement approach (Scoppe, 1973).

Torque measurement techniques, which use either an angular deflection or shear stress/strain, can be divided into two major categories. In the first approach, the measurement is made by placing an external system such as a commercially available products (COTS) torquemeter or load dynamometer. In the second approach, an internal measurement unit such as using strain gauges and phase angle shift is applied directly on the shaft. In operational engine applications, the internal torque measurement unit (TMU) is used because of the physical constraints such as geometry and weight. External TMUs such as dynamometers, COTS torquemeter are usually installed during development and

test phases to determine the actual torque output and check the internal torque measuring system (AGARD, 1994).

Aranson and Nelson mentioned a hydromechanical torque measuring unit assembled into the gearbox and uses hydraulic pressure difference to measure the torque in Torque Handbook (Aranson & Nelson, 1964). The power output shaft rotation is transmitted to planetary gear that is resisted by stationary ring spline as illustrated in Figure *3*. This resistance force causes an axial movement to the spring and plunger. The piston's movement forces the valve to open, thus increasing the flow of pressure oil into the chamber of the metering orifice. The pressure difference measured with a differential pressure transducer is proportional to the transmitted torque on the shaft. The measured hydraulic pressure difference is filtered and amplified for the engine control unit's data recording system (ECU) (Aranson & Nelson, 1964).

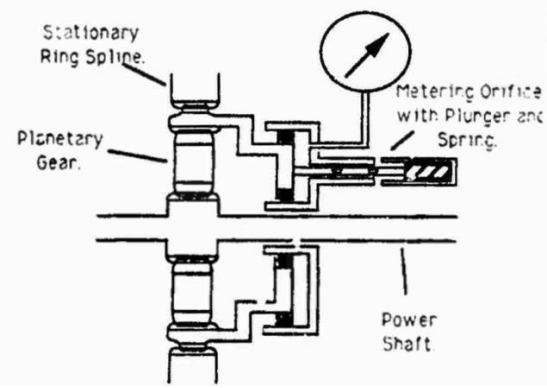

Figure 3. Hydromechanical torque measurement unit *(AGARD, 1994)*

The torsional strain is used by Steve Raymond and Douglas Baker by their invented TMU. A sensing unit can measure changes in surface strain, which is piezoresistive strain gages. They are attached to the outer surface of the output drive shaft, as shown in Figure *4*. The change in torsional strain is generally too small to be accurately measured directly. Therefore, the common practice is to use four strain gauges arranged in the Wheatstone bridge circuit. The shaft's twisting causes an unbalance in the bridge circuit, which is electrically coupled to the reporting unit by lead wires. The lead wires and strain gauges are covered in protective film to prevent damage during operation at high speed and temperatures. The reporting unit mounted at the end of the shaft configured the torsional

strain to report the central control unit to ECU. Excitation power is supplied to the system through either slip rings or transformer couplings (US Patent No. 7698959, 2010).

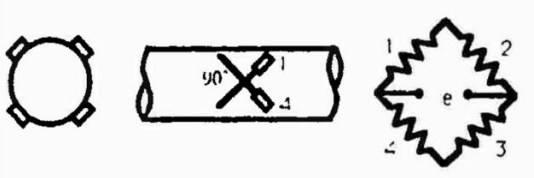

Figure 4. Strain-gauge torque measurement unit *(US Patent No. 7698959, 2010)*

On the other hand, Acker invented a TMU that does not use any physical response of power shafts such as shear stress, strain, or twisting angle. In this system, differential gas pressure is measured across the power turbine to generate a torque signal. The pressure taps are used to read the expanding gas, firstly as the gas travels from the gas-generating turbine to the power turbine inlet and secondly at the exit of the power turbine while the gas escapes through the exhaust port. The pressure difference between the two is used as input to a processor that also takes the power turbine's rotational speed, initial air pressure, and temperature. The processor results in various engine parameters, including the required output torque (United States Patent No. 7051535, 2006).

1.1.1. Angular Twist Method for TMU

One of the most common torque measurement methods in compact turboshaft engines is using an angular twist of the power shaft. There are various applications for determining the twist angle, depending on the system's configuration and design. After the signal is generated by the sensing condition unit (mostly an electromagnetic sensor but also an optical sensor that can be used), it is filtered and amplified. ECU then processes the signal to torque value illustrated by the torque indicator in Figure *5* (AGARD, 1994).

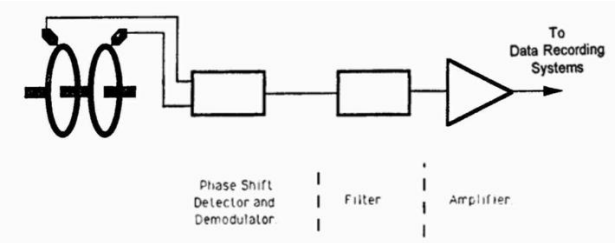

Figure 5. Angular twist torque measurement unit *(AGARD, 1994)*

The angular twist method generally requires a shaft and a feature, which is magnetizable and can be sensed by an electromagnetic sensor. It is common to design the feature in tooth shape. Thus as teeth pass through the sensor, they are easily recognized. The design and location of teeth can differ from application to application. Whereas one tooth is attached to the shaft's slender portion, the other one can be either located on the opposite end of the shaft or mounted on a ring or reference shaft assembled to the shaft. Two teeth-sensing units are required in applications where teeth are located on the shaft's front and rear parts. The magnetic sensor generates signals whenever the teeth pass through the electromagnetic field. Signals are electronic pulses shaped like sinusoidal waves, as illustrated in Figure 6. The timing differential of teeth causes the phase shift between signals. Torque transmission leads to phase shift changes that are computed to a relative twisting angle between the teeth. The relative twisting angle is processed by ECU to the torque value by an algorithm using torque versus twisting angle mapping (US Patent No. US8549931, 2013).

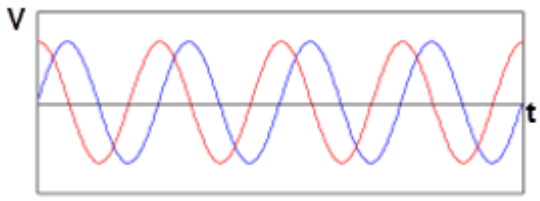

Figure 6. Electronic pulses of torque sensor

The old hydro mechanical torque measurement unit of a turboshaft engine of Motor Sich, Joint Stock Company, is replaced by a TMU that uses the angular twist method to measure the torque more accurately in real-time application. Mechanical parts of torque measuring unit shaft (power shaft), a screen, and an inducer (ring) are illustrated in Figure *7*. The screen is mounted on the shaft via tight fit, and it is pinned to the shaft from side A. There

is a small clearance between the shaft and the screen at side B; thus, torque is not transmitted on the screen. Inducer (ring) is mounted on the shaft. Both inducer and screen have eight identical equally spaced teeth. Note that there is a mounting angle between the teeth. During torque transmission, side A of the shaft is twisted relative to side B at an angle, a relative twisting angle, and proportional to the torque amount. As there is no torque transmission on screen, the shaft teeth are relatively twisted at some angle to the screen's teeth, so the mounting angle between the teeth is changed (Sirenko, Yepifanov, Podgorsky, & Nechunaev, 2018). The mounting angle change is determined to form the electromagnetic sensor signal, and it is processed to the transmitted torque value.

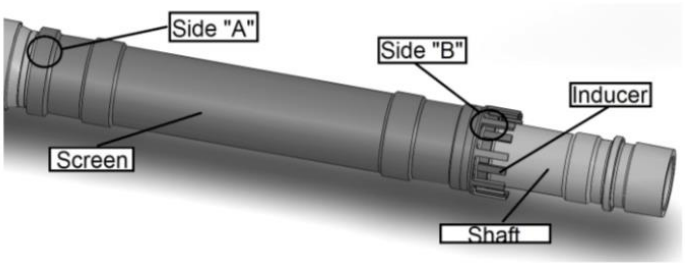

Figure 7. 3D model of torque measurement unit, Motor Sich *(Sirenko, Yepifanov, Podgorsky, & Nechunaev, 2018)*

Like Motor Sich's turboshaft, TMU of T700 turboshaft engine of General Electric (GE) Company uses the same basis of angular twist method. T700 turboshaft is one of the world's most demanding engine for the civilian and military application with a sold number of 20,000 and more than 100 million flight hours in nearly four decades of service. T700 engine has different configurations, and it produces an average of 2000 shp. Its major components consist of an inlet section, five stages axial and 1 stage centrifugal compressor, combustion chamber, 2 stage gas generator turbine, 2 stage power turbine, and exhaust frame together with the various accessories mounted on the forward and aft casings (see *Figure 8. GE T700 Turboshaft Engine*) (Aviation, 2020).

Figure 8. GE T700 Turboshaft Engine *(Aviation, 2020)*

Unlike Motor Sich's turboshafts TMU, a pinned reference shaft from the front end of the power shaft but free from the aft end allows the reference shaft to rotate relative to the power shaft. There is no torque transmission on the reference shaft. Both the power shaft and inside reference shaft have similar teeth feature as illustrated in *Figure 9*. The transmitted torque on the output power shaft results in a twist that causes the teeth on the power shaft to vary in position relative to the reference shaft's teeth. It leads to a change in the timing differential of teeth as they transpass through the torque sensor. Additional to the torque sensor, there is an rpm sensor (Np sensor) that measures the power shaft's rotating velocity. Both rpm sensor and torque sensor are electromagnetic, and they are back up to each other. The phase shift of the torque sensor's signal output is processed to the transmitted torque value by ECU (US Army Aviation, 2007).

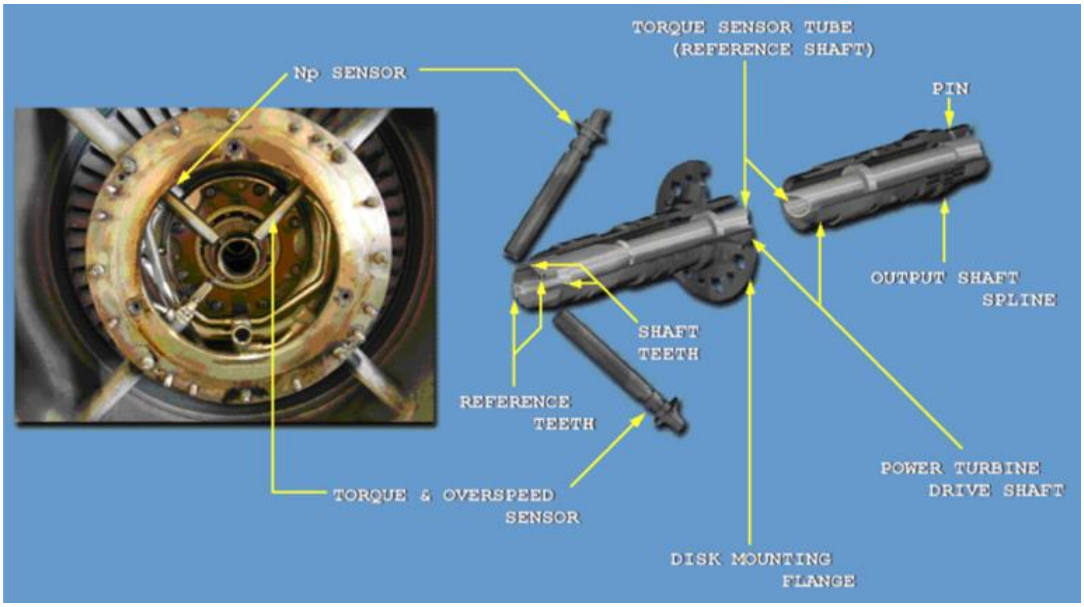

Figure 9. T700 Turboshaft Engine Torque Measurement Unit *(US Army Aviation, 2007)*

TMU of RTM 322 turboshaft engine of Turbomeca and Rolls-Royce joint company also uses the same angular twist method. Its TMU has a similar mechanical design to the GE T700 turboshaft engine's TMU. There is a reference shaft inside the power output shaft called a torquemeter, as illustrated in *Figure 10*. Torque signal is processed to torque value by full authority digital engine control (FADEC). RTM 322 firstly entered in service in 1995 and has over 1 million operating hours. It is one of the most favorite turboshaft engines in the European rotorcraft market. The engine has a compact modular configuration with three stages axial and one centrifugal compressor, a reverse flow combustion chamber, a two-stage gas generator turbine, and a two-stage power turbine (Lewis & Buller, 1985) and (Engines, 2020).

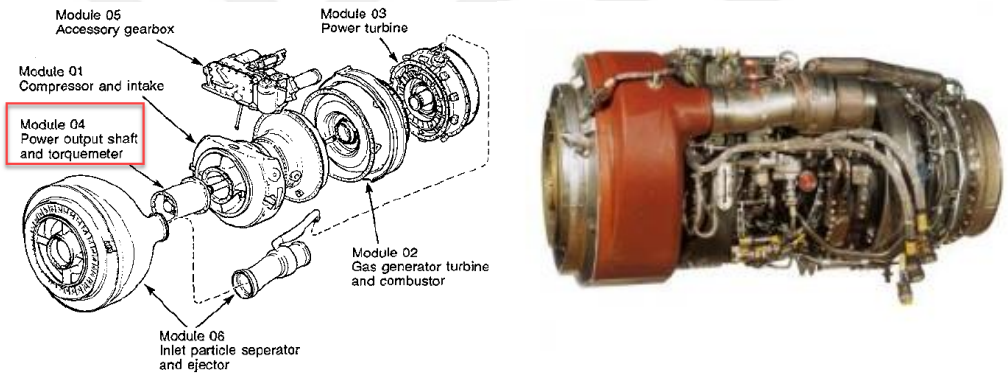

Figure 10. RTM 322 Turboshaft Engine Layout *(Lewis & Buller, 1985), (Engines, 2020)*

Another turboshaft engine, T800 of The Light Helicopter Turbine Engine Company (LHTEC), has a TMU with a similar angular twist method since the engine has a reference shaft inside the power output shaft. Though Becker D. and Frounfelker B. do not highlight it, Figure *11* illustrates the engine layout, where there is a reference shaft inside the output shaft, but different from T700, it is pinned from the aft side of the shaft and free from the front side. The reference shaft holds a blade-like feature, which should be recognized by a torque sensor, and a similar one should be on the shaft itself according to the same working principle of the angular twist method. T800 turboshaft engine produces 1300 shp and has a modular design. The engine core consists of a two-stage centrifugal compressor, a reverse flow combustor, a two-stage gas generator, and a two-stage power turbine

(Becker & Frounfelker, 1992).

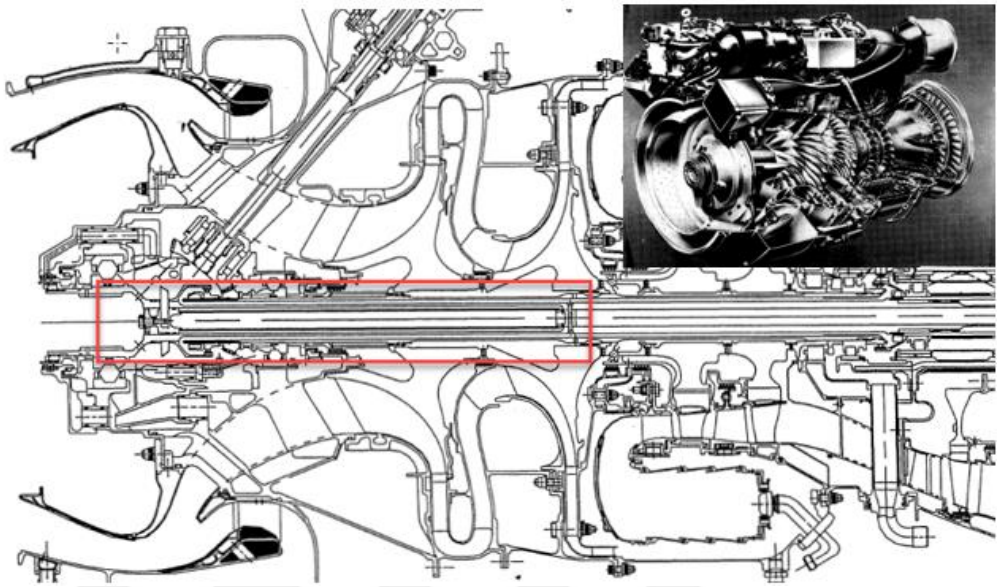

Figure 11. LHTEC T800 Turboshaft Engine *(Becker & Frounfelker, 1992)*

The angular twist method is a multidisciplinary approach with a strong base in mechanics, electronics, and control. The comparison of TMUs of benchmark turboshaft engines is made only according to the mechanical design aspect. In this thesis, the generic reference shaft of an alternative TMU for a turboshaft engine will be analyzed and tested. Similar reference shaft geometry with T800 and T700 turboshaft engines will be reengineered. The concept decision, the TMU reference shaft configuration, and design criteria will be explained in detail in the conceptual design part. In the analysis part, the reference shaft's mechanical integrity will be analyzed in terms of strength. Under vibration criteria, modal analysis and hammer tests will be performed to validate the design. Finally, the overall precision of the TMU and the need for calibration will be discussed in the future work part.

2. CONCEPTUAL DESIGN

The main goal of the TMU reference shaft (also named as torquemeter) is to behave as a reference point for torque measurement inside the power output shaft. Figure *12* shows the T800 engine reference shaft's details that carries a sensor blade tightened by a locking bolt. T800 engine reference shaft is fixed to the power output shaft by a pin from the aft side of the engine and free from the front side. An O-ring is on the front side to hinder the oil leakage between the reference shaft and power output shaft.

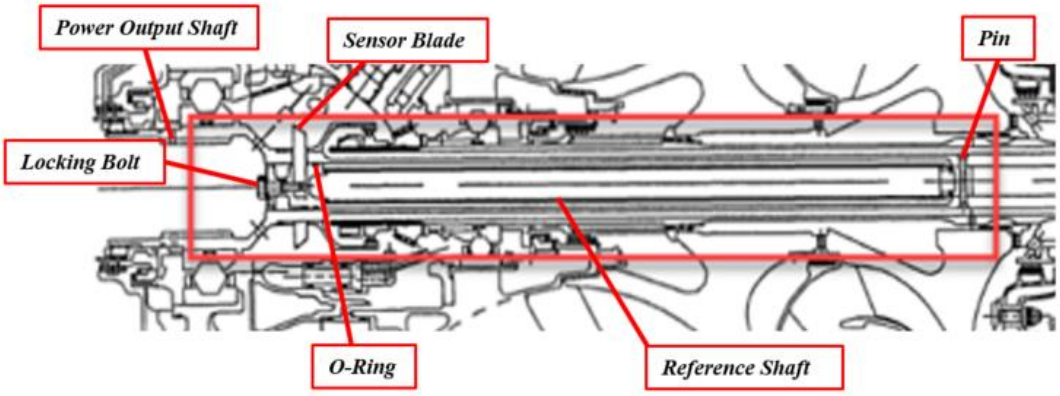

Figure 12 T800 Reference Shaft Geometry *(Becker & Frounfelker, 1992)*

Figure 13 shows the T700 engine reference shaft's details in the tube form, but differently, reference shaft is fixed from the engine's front side by a pin, and it does not carry a sensor blade; instead, it has machined reference teeth on it. Furthermore, it has two machined middle rings on it in case of contact with the power output shaft.

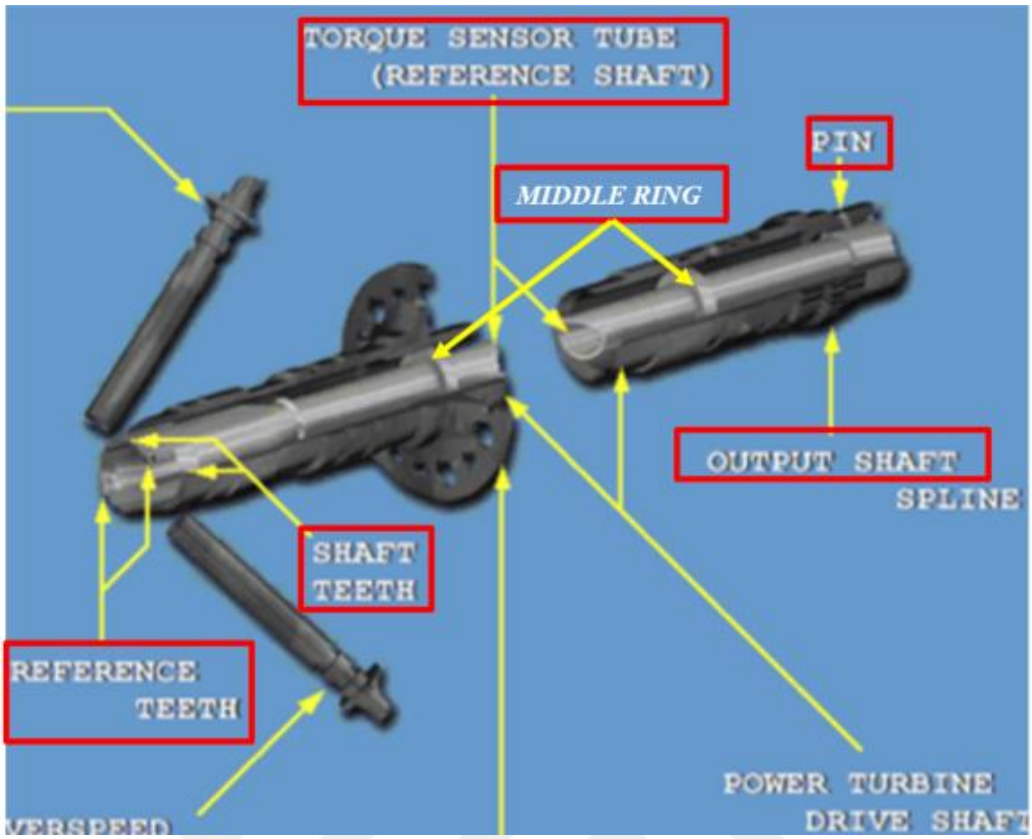

Figure 13 T700 Reference Shaft Geometry *(US Army Aviation, 2007)*

In this thesis, the reference shaft will be referred to as torquemeter, not to be confused with the power output shaft. In this conceptual design of generic torquemeter T800 and T700 reference shafts, geometries are used as guidance. However, the torquemeter possesses similar and different design features from both, and it has advantages and disadvantages comparing to them. The conceptual design of the torquemeter is illustrated in Figure *14*. Differently, it is aimed to be used for different power output shafts with minor modifications as an advantage. Therefore, it has modules that are the front ring, aft ring, middle rings, and tube. The modular design of the torquemeter allows it to be adaptive for different turboshaft engines as the total length of the torquemeter, which is (l) shown in Figure *14*, and the wall thickness of the tube, which is (d) shown in Figure 15, can be designed according to the power output shaft geometry with minor modifications on the tube. The total length of the torquemeter (l) can be changed easily with the tube length.

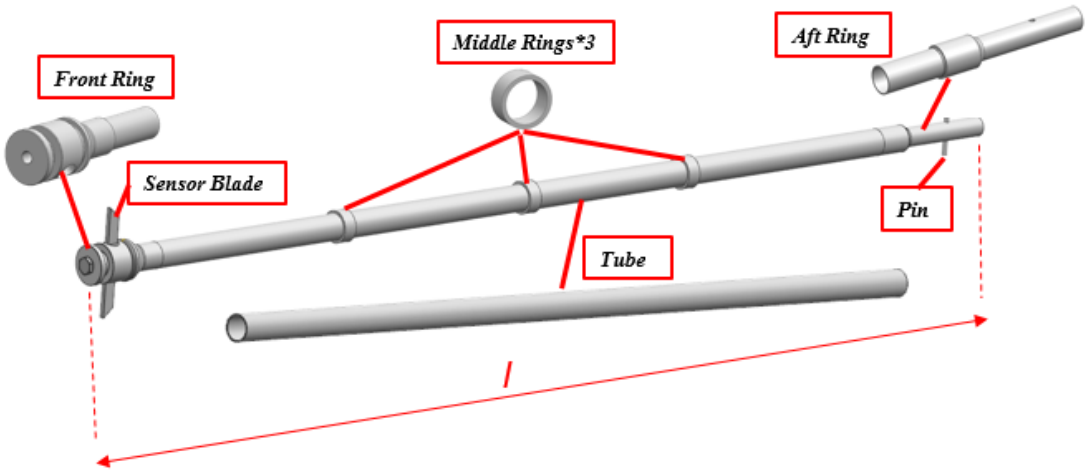

Figure 14 3D Model of Torquemeter (Reference Shaft)

The conceptual design needs to be manufacturable, easily assembled and disassembled, and lightweight. Bar and tube material form is selected, wider geometric tolerances are allowed if the tight tolerances are not required, and sharp edges are not allowed to be machined easily. Like T700, the need for tube form material originates from the weight concern so that the torquemeter can achieve lightweight design criterion. There is butt-welding between both the front ring and tube and the aft ring and tube. The torquemeter material shall be weldable to have a manufacturable design. Different from T700, three middle rings are mounted on the tube via intermittent welding. The middle rings are designed to have the first contact, if required, with the power output shaft rather than the tube. The middle rings' axial locations are selected according to the maximum radial deformation locations because of resonance elaborated in the analysis part. The radial clearance between the power shaft and middle rings can be controlled by the tube's wall thickness, rings, and the shaft's inner diameter. The modular design of the torquemeter requires using of welding joints; however, they cause disadvantages. Firstly, the welding process results decrease in the physical material properties such as yield strength. Secondly, the torquemeter becomes an inseparable assembly after welding is done. Finally, it creates residual stresses on the surface of the torquemeter that are undesired in terms of strength criterion. However, the torquemeter shall not fail under static and dynamic loads; these strength and vibration criteria will be elaborated detailed in the analysis part.

The 3D model and cross-section of the front side of the torquemeter are shown in Figure 15, which illustrates the torquemeter front ring's details. Like T800, the sensor blade is assembled on the front side, and a bolt provides the sensor blade's locking mechanism. Differently, the sensor blade hole on the front ring, which has clearance fit with the sensor blade, allows the sensor blade to be easily assembled and disassembled. There are internal threads on the sensor blade bolthole. The bolt is tightened to be torqued to fix the sensor blade to the torquemeter.

The front side of the torquemeter operates in an oily environment since the power output shaft requires oil. Unlike T700 and T800, the front ring of the torquemeter has two housings; while one is designed to be a backup for oil leakage as an open cavity, and the other one is designed to be an O-ring groove. O-ring shall be selected according to operating conditions to hinder the oil leakage. The online O-ring calculator is used to calculate the O-ring size and its groove dimensions according to the international O-Ring Standart ISO 3601 (Trelleborg O-Ring Calculator, 2020). O-ring groove at Figure 15, which has an outer diameter (a), is machined according to the selected O-ring that has an inner diameter (o) (a/o is equal to 1.032). The O-ring's outer diameter and the gap between the torquemeter groove and the shaft are selected according to the shaft's inner diameter. Viton-70 material is selected for engine application. However, to examine O-ring's stiffness impact on natural frequencies, Viton-90 material is compared in the analysis part. The oil must not leak between the torquemeter and output power shaft as it can lead to coke formation because of temperature. Besides the oil fire risk, coking oil may lead to unbalance for both shaft and torquemeter.

The butt-welding leap design detail between the tube and front ring is shown as the butt weld region in Figure 15. The front ring has the leap feature that goes into the tube.

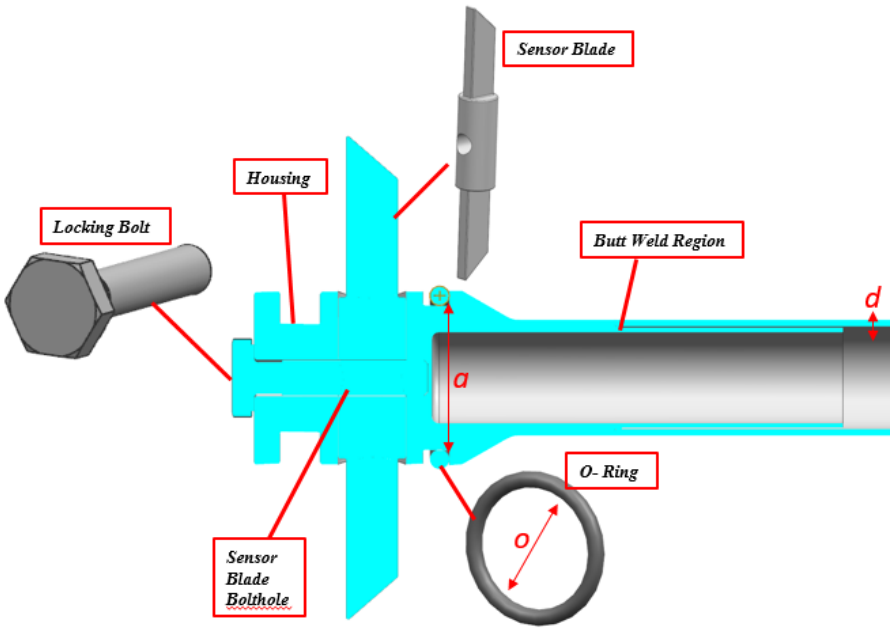

Figure 15 3D Model and Cross Section of the Torquemeter Front Side

The 3D model and cross-section of the aft ring are shown in Figure *16*. The leap design of butt-welding is illustrated similar to the front ring. Differently from T700 and T800, the aft ring geometry allows that torquemeter to be pushed or pulled inside the power shaft during assembly depending on the shaft's geometry. The power shaft can be drilled through lengthwise, or it has a slot inside for the torquemeter aft ring. The Torquemeter pinhole shown on the aft ring is drilled for the power shaft and torquemeter simultaneously during the assembly process. After drilling the pinhole, the pin is installed through this hole. As there is a diametrical interference press fit between the pin and the hole, both shall be oiled before the installation to achieve easily assembled design criteria. Furthermore, cooling the pin and heating the torquemeter with a power shaft will benefit the assembly's easiness. Eventually, this pin's assembly fixes the torquemeter to the power output shaft from the aft side.

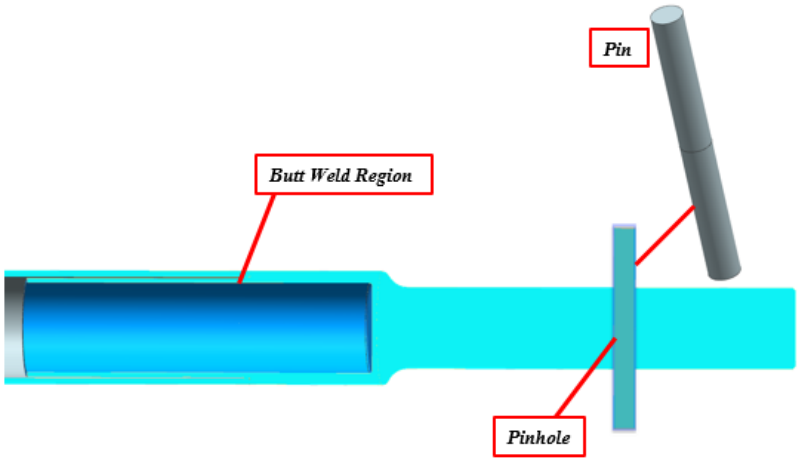

Figure 16 3D Model and Cross Section of the Aft Ring

Torquemeter concept design has to meet several design criteria to achieve its form, fit, and function. There is no torque transmission on the torquemeter, as it is fixed from the rear end to output power shaft via a pin; but free from the front side. Torquemeter carries the sensor blade that is assembled to the front side. Sensor blade material requires having magnetic properties, as an electromagnetic sensor shall recognize it for torque measurement. The power output shaft is twisted as a physical response proportional to the torque amount that acts on it. The power output shaft has a feature having an identical shape with the sensor blade that is named as the tooth. This tooth is either assembled on a shaft similar to Motor Sich power shaft (Sirenko, Yepifanov, Podgorsky, & Nechunaev, 2018) or machined together with the power shaft similar to the case in T700 output shaft (US Army Aviation, 2007). Because of the twisting of the power output shaft, the tooth on the shaft varies in position relative to the sensor blade. The change on the mounting angle between the tooth and sensor blade is processed as a phase difference from the generated torque sensor signal, and it is converted to the torque value by ECU.

3. ANALYSIS

The torquemeter has to sustain its mechanical integrity under static and dynamic loads. Therefore, it has design criteria for strength and vibration. Strength criterion is applied according to static structural analysis that the equivalent stresses on torquemeter shall be less than a minimum 0.2 % offset Yield Strength. Also, special attention shall be paid to welding locations because of residual stresses. The equivalent stresses, including residual stress on welding joints shall be less than 85 % of the 0.2 % offset Yield Strength by design practice. Vibration criterion is applied according to modal analysis that there shall not be any crossing, which is a coincidence of the natural frequencies of the torquemeter with engine operational frequency range, within the ± 10 % of the turboshaft engine operational speed to avoid resonance and destructive vibration by design practice. Firstly, modal analysis at free-free condition is validated by the hammer test, and then the prestressed modal analysis is run with the same geometry to show compliance with the vibration criteria.

The finite element software *'Ansys Workbench v.19.2'* is used for the analyses. There is no external loading on the torquemeter other than thermal, rotational, and gravitational causes. Thermal mapping of the torquemeter is assumed from the turboshaft engine steady-state operation condition according to the bearing temperatures and shaft temperature of the T800 that is also specified to be INCO718 (Becker & Frounfelker, 1992) and (Douglas, 1991). Steady-state engine output speed is used as 23,000 rpm accordingly to the LHTEC T800 Engine EASA Type Certificate datasheet. (EASA, 2008)

3.1. Static Structural Analysis Preprocessing

Strength analysis is the basis of structural design that ensures a component meets its necessary fit, form, and function requirements. Finite element analysis (FEA) is applied to predict a structure's failure to the applied loads (in the static analysis, the load is not time-dependent).

Static structural analysis is selected from the analysis systems toolbox. Material selection of the torquemeter is made as nickel-based alloy and steels accordingly, INCO718 for the torquemeter, AM355 for the Sensor Blade, the locking bolt, and the pin from INCO718 ((MatWeb, 2011)). Nickel-based alloys are selected since they are very resistant to oxidation and corrosion. They are ductile, and they retain their strength over a wide range of temperatures. It leads them to be highly preferred, particularly in a high-temperature application such as GTEs and the nuclear industry, because of their durability (Morinaga, 2018). Furthermore, INCO718 alloy has outstanding weldability desired for torquemeter material, and AM355 steel has magnetic material properties and durability that makes it attractive for the sensor blade.

The geometry, including the solid models of the torquemeter, sensor blade, locking bolt, and pin, is imported as CAD data .prt into Ansys Design Modular, elaborated in the conceptual design section. The modeled geometry has the total length (l) that is considered as reference length. All other dimensions are normalized with respect to the reference length, so modeled geometry has the total length (l) of 1.00, and tube wall thickness is (d) 0.0025.

For the coordinate system, cartesian *x*, *y*, and *z* global coordinates are selected, as illustrated in Figure *17*.

Figure 17 Coordinate System & Geometry

Connection types between the parts in the analysis are selected accordingly below in Figure *18*. Contact faces are highlighted in red color, and target faces are highlighted in blue color. The friction coefficient value of 0.11 is used according to hardened steel on hardened steel coefficient of friction with oil (Fuller, 1940). As there is an interference fit between the pin and the torquemeter, the offset for the frictional contact is set to a

normalized value of 0.00001 in the radius with respect to the total length.

1) Sensor Blade and Front Ring: Frictional Multiple to Multiple
2) Bolt and Sensor Blade: Bonded Solid to Bolt
3) Bolt and Front Ring: Frictional Bolt to Solid
4) Pin and Aft Ring: Frictional Multiple to Multiple

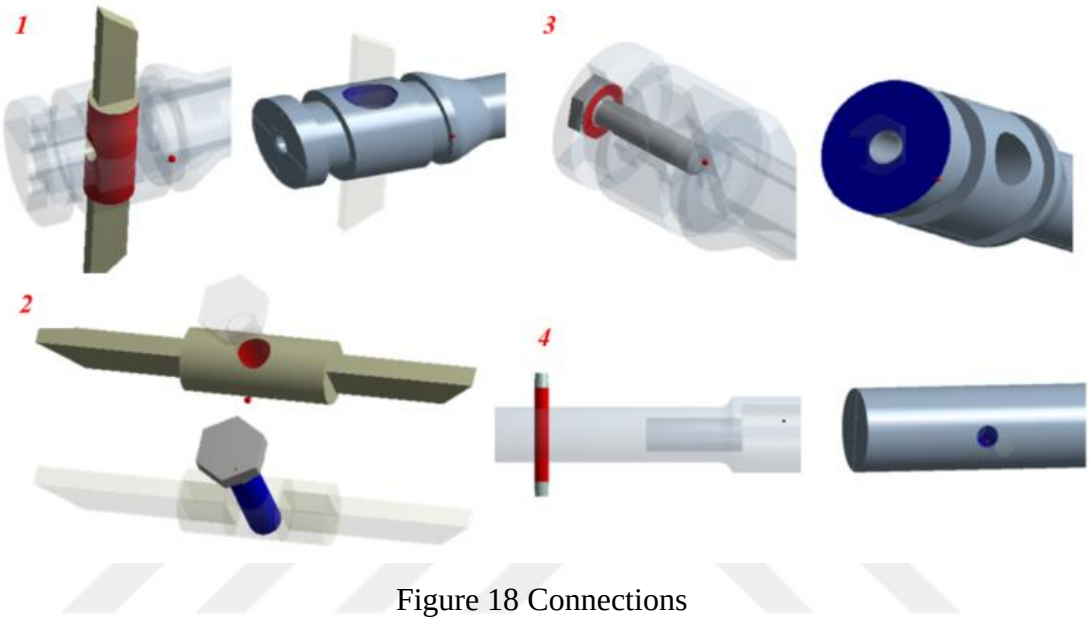

Figure 18 Connections

The remote point is added on the O-ring groove surface, allowing the installation of boundary conditions to model O-ring radial stiffness. Then the ground bearing element in Figure 19 is used to add the stiffness of the O-ring. However, the stiffness of the selected rubber O-ring is not available from the specifications.

The selected O-ring's stiffness values are calculated according to the empirical study on elastomer O-rings (NASA, 1977). The study's objective is to use the test rig to provide elastomer O-rings' stiffness as radial bearing mounts. Empirical results are given for different materials, including Viton-90 and Viton-70, which is Torquemeter O-ring material. In the paper, empirical test data is used to have a general algebraic expression for design and comparative purposes. The algebraic equation for stiffness is given in Eq. (3), where k is for stiffness in N/mm and f is for operational frequency in Hz. A and B are stiffness coefficients from empirical data depending on the material, operation temperature, squeeze percentage of the O-ring.

$$k = A\,(2\pi f)^B \tag{3}$$

Firstly, *A* and *B* coefficients are selected for Viton-70 and nominal operation conditions from Table-6 given in the paper (NASA, 1977). Then stiffness value *k* is calculated as 5500 N/mm for *f* is equal to 383.33 Hz (23,000 rpm) that is the operational frequency of the torquemeter.

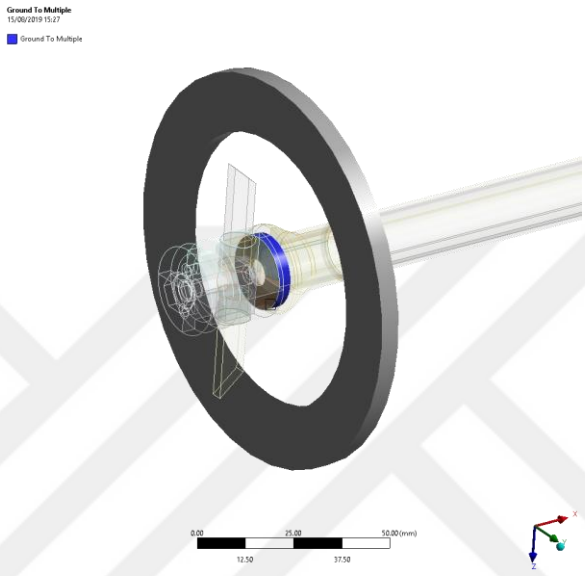

Figure 19 Ground Bearing Element

The meshing of the torquemeter geometry is done accordingly in Figure 20. To indicate the validation of the used element number and mesh independence, mesh convergence is given in Figure 21. Mesh convergence is done by using adaptive mesh refinement under solution. The maximum refinement loops and refinement depth is set to 3. After inserting equivalent stresses (Von-Mises) from the stress section, convergence is inserted for stress history. Under details of convergence, the type is selected as a maximum to indicate the change in maximum stress, and the allowable change in stress is less than 0.1 %.

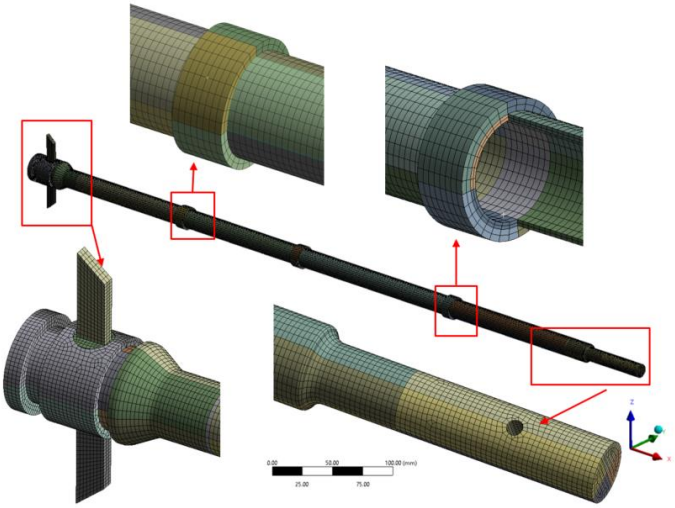

Figure 20 Meshed Geometry of the Torquemeter

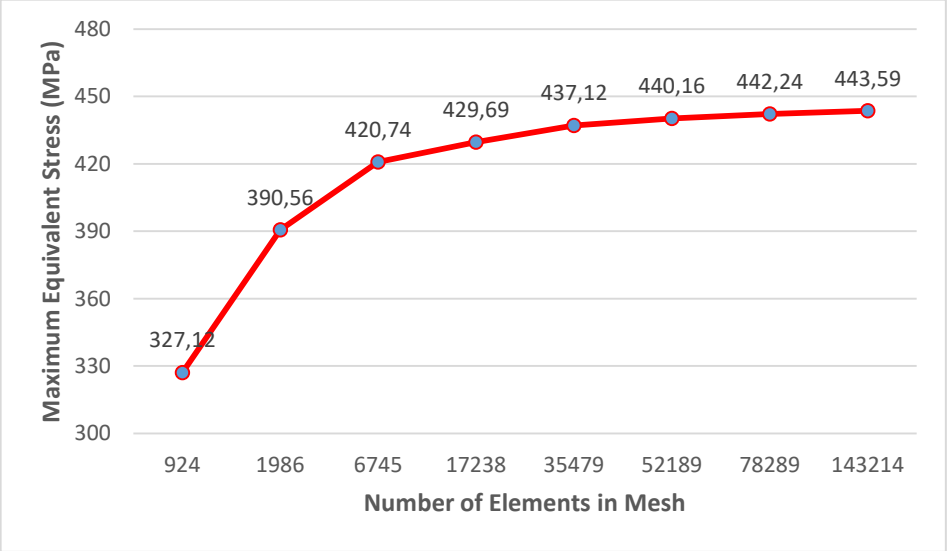

Figure 21 Mesh Convergence

In Figure 21, the stress results line becomes almost horizontal. It indicates that variation on stress results is close to zero (the last change on stress is 0.30 %), and mesh independence is met.

- All quadratic elements are used (SOLID186, SOLID187)
- Total element number is 143,214
- Total node number is 654,278
- Two quadratic elements per pipe thickness are created
- Sweep, patch conforming and hex dominant methods are used
- Body, face and edge sizing are done

Standard Earth Gravity is added -9806.6 mm/s^2 in the **z**-direction. Rotational velocity is implemented around the *x*-direction as 23,000 rpm for the turboshaft engine steady-state operational velocity.

Cylindrical support is inserted for the pin because it has a cylindrical surface. Cylindrical support allows the pin to move along its axial and radial axes because of interference fit and thermal growth, but it is fixed along the tangential direction.

The thermal condition of the torquemeter is generated by using steady-state thermal linear interpolation from analysis systems, as illustrated in Figure 22. It is assumed according to the turboshaft engine steady-state operation of the T800 (Becker & Frounfelker, 1992) and (Douglas, 1991), where the maximum bearing temperature of the T800 engine is on the rear side that is equal to 270°C whereas minimum bearing temperature is on the front side that is equal to 177°C.

Figure 22 Thermal Condition

The locking bolt is assumed to be tightened to torque with 5 Nm equal to nominal 7100 N preload, added as bolt pretension.

In analysis settings, the number of steps is set to 1, which is the load step. It applies all defined loads simultaneously: gravitational and rotational caused ones, thermal load, and the bolt's pretension. Under solver control, the solver type is selected as iterative using an iterative process called the Newton-Raphson Method. A large deflection option is enabled to calculate the true stresses and strain. Under output control, stress and strain options are enabled to indicate the results.

3.2.**Static Structural Analysis Solution**

The limit load is defined as the maximum load that is experienced throughout the operating range. In the preprocessing section, loads are defined for the torquemeter, so there are no external loads on the torquemeter other than gravitational, thermal, and rotational forces. Also, the interference fit is defined, and the bolt pretension is included.

Strength criterion as defined above in the preprocessing section that the equivalent stresses (Von-Mises) on torquemeter shall be less than minimum 0.2 % offset Yield Strength because the structure must not suffer permanent detrimental deformation under limit loads and must not rupture. In the static structural FEA solution, one can easily insert equivalent stresses (Von-Mises) from the stress section and solve it.

The results are given in Figure *23* and Figure *24* that illustrate the maximum and minimum equivalent stresses on the Torquemeter. The maximum equivalent stress is equal to 443.59 MPa that is around the pinhole. The 0.2 % offset Yield Strength of the INCO718 is equal to 1100 MPa at 23°C, and it is equal to 980 MPa at 650°C (MatWeb, 2011). However, the maximum temperature on torquemeter is equal to 270°C, 980 MPa is used for the 0.2 % offset Yield Strength of the INCO718 to be on the conservative side. Comparing the maximum equivalent stress on Torquemeter to 0.2 %, offset Yield Strength of the INCO718 indicates that strength criteria is met.

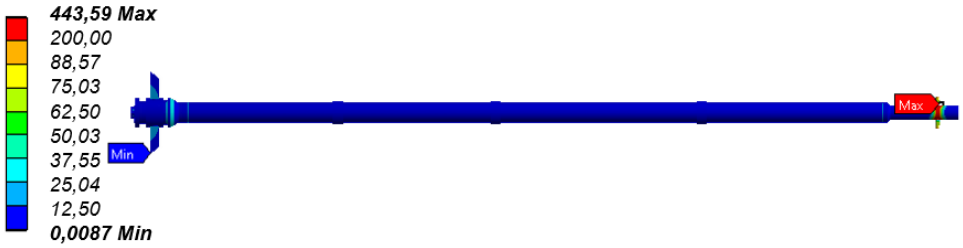

Figure 23 Max and Min Equivalent Stresses on Torquemeter

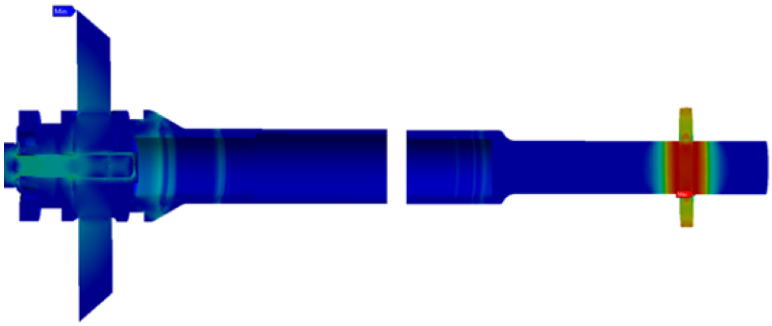

Figure 24 Equivalent Stresses on Cross Section

Furthermore, the factor of safety (FOS) is the division of the 0.2% offset Yield Strength by the maximum stress at applied loads. Based on the performed analysis, the FOS of the Torquemeter is calculated as 2.20 that indicates over safe design because the structure can withstand static loads with FOS between 1.25 and 2.00 (Dobrovolsky & Zablonsky, 1978).

The strength design criterion additionally requires that the equivalent stresses, including residual stress on welding joints shall be less than 85 % of the 0.2% offset Yield Strength by design practice because the welding process decreases the material properties such as Yield Strength and the residual stresses can significantly affect the performance.

Residual stresses are defined as the stresses that remain in a structure after manufacturing and processing in the absence of external forces or thermal gradients. Residual stresses can be tensile or compressive. Residual stresses are beneficial when they operate in the plane of the applied load and are opposite in a sense (for example, compressive residual stress in a component subjected to an applied tensile load). Tensile residual stresses on the surface of a structure are generally undesirable since they can contribute to a failure. Welding residual stresses are caused by differential thermal expansion and contraction of the weld metal and parent material. Residual stress levels on weld center and heat-affected zone (HAZ) can be very high tensile stresses. Therefore, it is critical to measure the residual stress when welding is applied during the manufacturing process (Kandil, Lord, & T., 2001) & (Suominen, Khurshid, & Parantainen, 2013).

The most important way to control and analyze residual stresses is to measure them through different ways such as hole drilling, X-ray diffraction (XRD), curvature,

ultrasonic methods, and neutron diffraction. To investigate the residual stress levels on the surface of the Torquemeter because of welding, XRD is used as it is accurate, relatively cost-effective, and available for laboratory testing. Residual stress measurement is done via X-ray diffractometer Xstress G2R that is non-destructive and suitable for laboratory. In the XRD method, the elastic strain is measured using Bragg's law, and the calculation of the stress is done with Hooke's law together with elastic modulus and Poisson's ratio. Any stress, including applied and residual stresses, causes a strain that corresponds to crystal lattice spacing changes. Bragg's law describes X-ray diffraction from crystal lattice planes in Figure *25*. In a stressed material, the wavelength of the X-ray (λ) is known, the distance between atomic planes (d) is unknown, and the diffractions are observed at angles (θ). Stress causes small changes in d and shifts the diffraction angle. Residual stresses are determined from the diffraction data by calculating the strain from the diffraction peak positions (Stresstech, 2020).

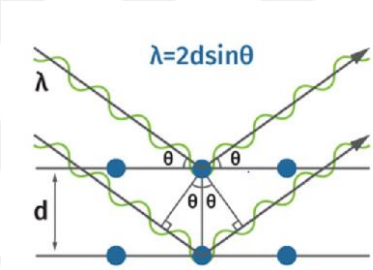

Figure 25 Bragg's Law

Test specimens are manufactured using the same welding process for butt welding and intermittent welding of the Torquemeter given in Figure *26*. Five test specimens are used for each welding region because of accuracy. Measurement is done for three defined points around the weld center and HAZ that are detected by XRD. Chromium (Cr) X-ray tube is used for INCO718 material.

Figure 26 Test Specimen for XRD Measurement

By rotating the X-ray diffractometer's goniometer between 0°, 45° and 90° directions, stress values are detected, and stress tensors are provided. The stresses on the weld center are higher compared to stresses on HAZ, resulting in tension. Only maximum stresses among the measurements are used in the stress tensor to be on the safe side. However, the change between the measurements is below 20% caused because of the grain size variations around the welding center. Stress tensors for butt weld and intermittent weld region are given in Table 1, where stresses are in MPa. Furthermore, equivalent stresses (σ_{eq}) (Von-Mises) are calculated according to Eq. (4).

$$\sigma_{eq} = \sqrt{\left[\left(\frac{(\sigma_{11}-\sigma_{22})^2+(\sigma_{22}-\sigma_{33})^2+(\sigma_{33}-\sigma_{11})^2}{2}\right) + 3({\sigma_{12}}^2 + {\sigma_{23}}^2 + {\sigma_{31}}^2)\right]} \quad (4)$$

Table 1 Stress Tensors

Butt Weld Region Weld Center Stress Tensor			**Intermittent Weld Region Weld Center Stress Tensor**		
443.7	-26.7	7.7	-45.3	53.8	50.5
-26.7	154.8	100.3	53.8	292.3	23.3
7.7	100.3	0	50.5	23.3	0
Equivalent Stress: 429.70 MPa			**Equivalent Stress: 344.52 MPa**		

Figure *27* indicates the welding joints between the front ring and the tube that is butt-welding, between the first middle ring and the tube that is intermitting welding. The maximum equivalent stress on the butt weld region is equal to 15.48 MPa and it is 4.72 MPa on the intermittent weld region.

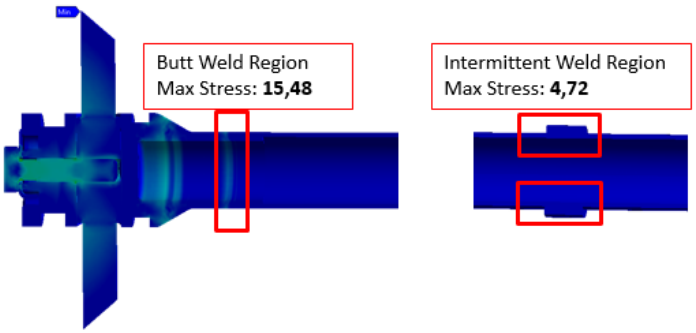

Figure 27 Equivalent Stresses on Welding Joints-1

Figure *28* indicates the welding joints between the aft ring and the tube that is butt-welding, between the third middle ring and the tube that is intermitting welding. The maximum stress butt weld region is equal to 10.32 MPa and it is equal to 5.83 MPa on intermittent weld region.

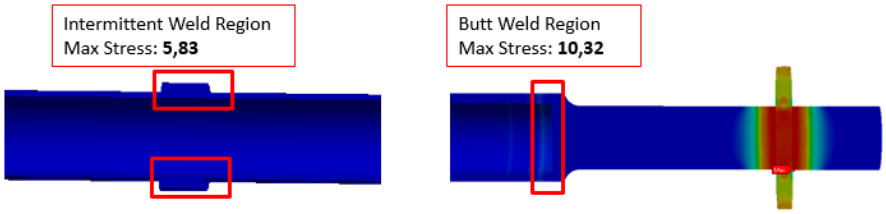

Figure 28 Equivalent Stresses on Welding Joints-2

The maximum equivalent stress on the butt welding joint is 15.48 MPa from FEA, and the maximum calculated residual stress on the butt weld region is 429.70 MPa via XRD measurement. The equivalent stress, including residual stress on the welding joint, is 445.18 MPa that is less than 85 % of the 0.2% Yield Strength, 833 MPa. It indicates that the strength design criteria for residual stresses are met. As the stresses on the intermittent weld region from both FEA and XRD measurement are less than the butt weld region's stresses, the design criterion is also met for intermittent weld joints.

Furthermore, FOS for welding joint is calculated as 1.86 that indicates safe design because it can withstand static loads with FOS between 1.25 and 2.00 (Dobrovolsky & Zablonsky, 1978).

3.3. Modal Analysis and Location of the Middle Rings

The modal analysis provides critical and valuable inputs for determining and managing the design parameters, such as vibration characteristics. It analyzes the dynamic properties of the structure in the frequency domain that indicates the structure's movement under dynamic loads. Modal analysis output provides natural frequencies and mode shapes of a mechanical structure. All structures have natural frequencies at which structure tends to vibrate when it is somehow disturbed, such as hitting and strumming. The mode shapes illustrate the structure's deformation would show when it vibrates at a natural frequency (resonance). Natural frequencies and mode shapes are not inherent material property; they depend on geometry and boundary conditions. There are different types of modes, such as rigid body modes and flexible body modes. Six rigid body modes exist, three of them are translational, and the rest are rotational. Rigid body modes occur at zero because of low spring stiffness and not adequately supported structure. Flexible body modes can be categorized into three groups such as bending, torsional and axial modes.

Middle rings are designed to be the first contact point with the power output shaft, if required, rather than the torquemeter tube in case of resonance. Modal analysis is done to decide the axial location of middle rings because mode shapes indicate where maximum deformation occurs during resonance. The same model with the structural analysis given in Figure *17* is used, but the middle rings are excluded from deciding the axial location and comparing the effect of middle rings on natural frequencies. In the modal analysis, linear elastic material behavior is assumed. The required material properties such as density, Young's modulus, and Poisson's ratio for modal analysis are imported from MatWeb (MatWeb, 2011). Contact regions are available in the modal analysis that is given in Figure 18. The choice of boundary conditions directly affects the structure's intention to vibrate, so its mode shapes and frequencies. The same boundary condition with the structural analysis is used that rotational velocity, thermal condition, and cylindrical support are inserted. The static structural analysis solution level is linked to the modal analysis setup level. The static structural analysis result becomes an initial condition for the modal analysis. After the solution is complete, the mode shapes and natural frequencies are provided. Mode shapes are given in Figure *29* that indicates the

first and second bending modes for the torquemeter. Total deformation is illustrated through colored counters that provide where the maximum deformation is red. The magnitudes on the resulting legend are relative deformation values. However, they are used to adjust the middle rings' axial location, where maximum deformation occurs.

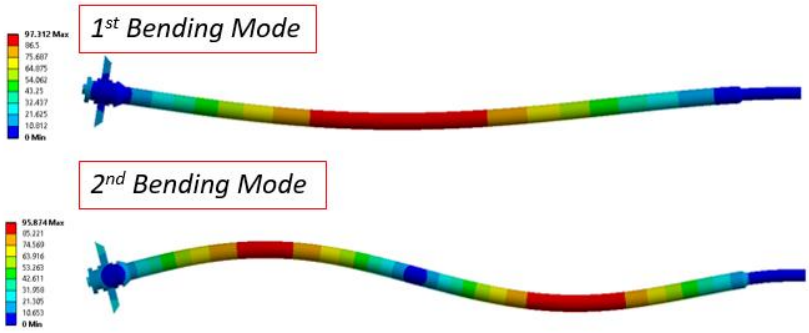

Figure 29 Mode Shapes for Middle Rings Location

In this paper, natural frequencies are normalized with respect to the first natural frequency result of the hammer impact test on the hanging configuration. The normalized natural frequencies of first and second bending modes are respectively 1.003 and 3.205 by excluding the middle rings from the model.

3.4.**Free-Free Modal Analysis**

Free-free modal analysis is done to validate the meshed geometry model with its material properties and connections via the impact hammer test by comparing their natural frequencies. There is no support and constraints used in the free-free modal analysis. Thermal and structural loads are not inserted. Temperature change affects the variation of material properties such as Young's modulus and Poisson's ratio. However, no temperature change for free-free modal analysis is applied at constant room temperature 23°C, so thermal mapping is not installed. In analysis settings, the maximum modes to find option is set to 10, and the limit search to range option is not enabled. Under solver control, the solver type is selected as iterative using an iterative process called the

Newton-Raphson Method.

When the solution is complete, the solution branch displays a bar chart and table listing natural frequencies and mode numbers given in Table *2*.

Table 2 Normalized Natural Frequencies of Free-Free Modal Analysis

Mode No.	Frequency
1	1.006
2	1.006
3	3.099
4	3.103
5	6.398
6	6.416
7	10.832
8	10.877
9	11.109
10	15.703

Mode shapes are given in Figure *30*, indicating deformation through colored counters from red (maximum) to blue (minimum), but the deformation magnitudes on the resulting legend are relative.

The first and second mode shapes are mode pairs. The first bending mode occurs at normalized natural frequency 1.006. Maximum deformation is close to the second middle ring and aft side of the torquemeter. Second and third mode shapes are mode pairs for the second bending mode with normalized natural frequencies 3.099 and 3.103; however, this difference is assumed to be due to Ansys' numerical errors. Maximum deformation is on the first and third middle ring.

Similarly, the fifth and sixth mode shapes are mode pairs for the third bending mode with normalized natural frequencies 6.398 and 6.416. Forth bending mode has similar relation for the seventh and eighth modes that are mode pairs with 10.832 and 10.877 normalized natural frequencies. Differently, the ninth mode shape is a torsional mode that has

normalized natural frequency 11.109.

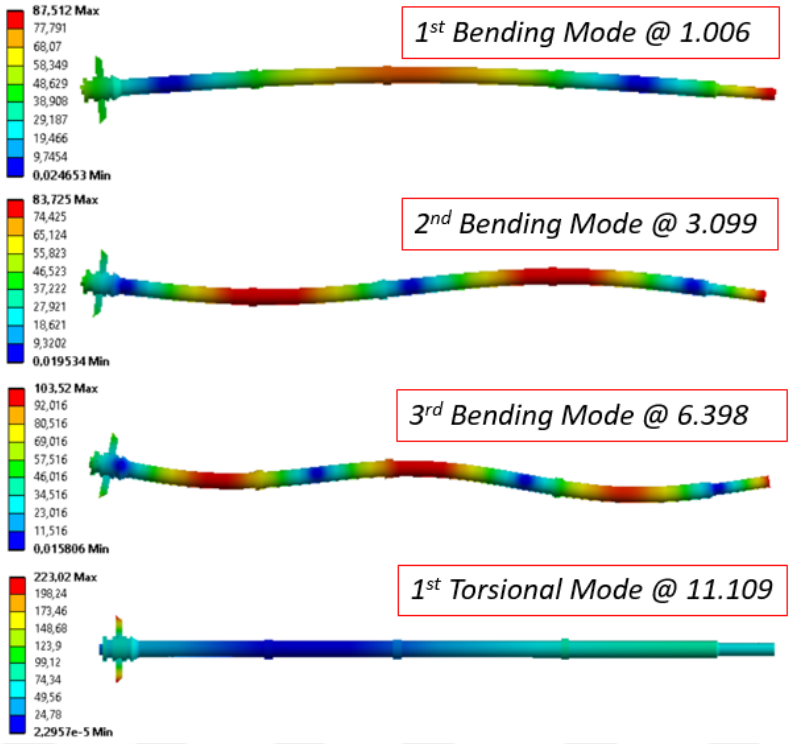

Figure 30 Mode Shapes of Free-Free Modal Analysis

3.5.**Hammer Impact Test**

The hammer impact test is the response of displacement, velocity, or acceleration of mechanical structure in return for a known force application. The mechanical structure is excited with an impact hammer, and an accelerometer records the response. The main advantage of the impact hammer test is the easiness of exciting the structure in a wide frequency range. The impact hammer test identifies natural frequencies, mode shapes, and modal damping values of the mechanical structure via frequency response function (FRF), a frequency-based measurement function. FRF is referred to as a transfer function between the input and output. The amplitude and phase of multiple FRFs to a common reference on a structure are used to determine complete mode shapes., The coherence function is examined to validate the outputs of the impact hammer test. The coherence function, which ranges between zero and one, provides the measurement quality of the FRF. A coherence function value, which is above the threshold value 0.9 at a particular

frequency, indicates that the FRF amplitude and phase are repeatable from measurement to measurement. On the other hand, a coherence value below the threshold value indicates a possible error in the measurement setup (Siemens, What is Frequency Response Function (FRF), 2020).

There are two common approaches in the impact hammer test: the Roving accelerometer and roving hammer. The roving accelerometer method is defined as a single input multiple outputs in that accelerometer location is changeable, but the location on where the hammer hit is fixed. The roving hammer method is defined as multiple input single output in that the location on where the hammer hit is changeable, but the accelerometer location is fixed. The choice to move either the accelerometer or the hammer between the measurement points may outwardly appear to be the same in terms of natural frequencies. However, there are advantages and disadvantages for both. The roving hammer method has some advantages over the roving accelerometer method. Moving the accelerometer requires dismantling and reassembly at different measurement points again, which leads to instrumentation difficulty. Though a lightweight accelerometer is used, a moving accelerometer on the structure changes the mass distribution that may affect natural frequencies. However, the moving hammer method is not without concern. As the hammer inputs in a single direction and a triaxle accelerometer measures output in three directions, it can result in incomplete mode shapes. (Siemens, Modal Tips: Roving Hammer versus Roving Accelerometer, 2019). The roving hammer method is selected to be applied for the impact hammer tests; however, a single axis accelerometer is enough because of the geometry of the torquemeter.

Equipment selection is an essential criterion for the accuracy of the impact hammer test. The main essential equipments are an accelerometer and impact hammer. The lightweight accelerometer is preferred not to affect the measured modes of the structure. Besides, the frequency response band of the accelerometer has to be compatible with the focused frequency range. For the Torquemeter impact hammer test, the PCB 352A73 model single-axis accelerometer, shown in Figure *31*, is selected as it is small in size, lightweight, and has high accuracy with a broad frequency range that is not to miss the modes of the Torquemeter. Likewise, the impact hammer shall support a high-frequency range that shall provide enough force not to miss the modes of the Torquemeter. The correct impact hammer shall ensure enough force is being inputted into the structure to

excite the full frequency range, which mainly depends on hammer mass and hammer stiffness. If the hammer is lightweight, it decreases when it is in contact with the structure that provides a short impact pulse and wide frequency range. Also, for lightweight structures like the Torquemeter, light hammer mass supply enough force as input. The stiffness of the impact hammer depends on tip material that is separable assembly. If the required frequencies are low, then soft tips are used, such as plastic, rubber, etc.; if not, then hard tips such as metal are used for actuating higher frequency. PCB 086E80 model, which is selected in Figure *31*, is selected for the Torquemeter impact hammer test.

Figure 31 The Accelerometer and Impact Hammer for the Torquemeter Test

The accelerometer is mounted at the tip of the aft ring because of the bending modes, where the aft ring is not the nodal point and easiness of the instrumentation surface. It shall be ensured that the accelerometer's measurement aligns with the global coordinates of the Torquemeter, so the Z direction channel of the accelerometer is facing down. According to the driving point search, fifteen measurement points are decided to be the impact hammer's excitation location given in Figure 33. The impact hammer and accelerometer are roved together over the torquemeter at the same location to identify the resonant frequencies. Each measurement point is excited for ten times by impact hammer to have repeatable and accurate measurements.

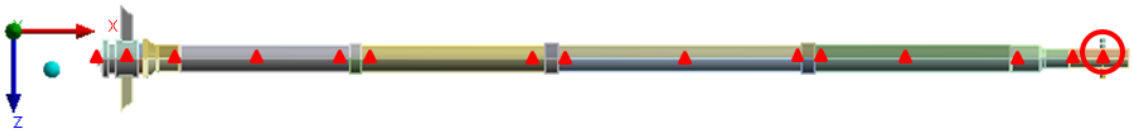

Figure 32 Accelerometer Location and Measurement Points

During the impact hammer test, LMS Test Lab17 Impact Testing Module software and

LMS Scadas Mobile Data Acquisition System has been used.

The impact hammer test is applied at two different configurations to simulate the free-free boundary condition for modal analysis. The first is hanging the Torquemeter with elastic ropes from the fixed bar, and the second orientation is on a foam rubber fixture. Both configurations are illustrated in Figure *33*.

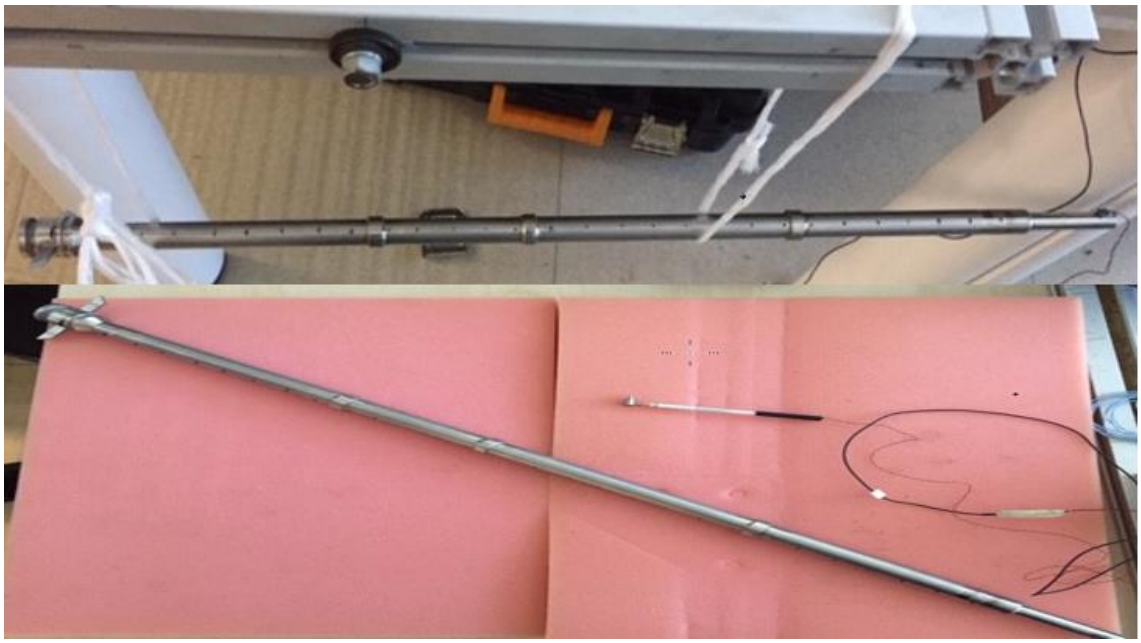

Figure 33 The Impact Hammer Test Configurations for the Torquemeter

A short impact pulse in the time domain is desired for a broader excitation frequency domain response. Input force graph of the impact hammer is given in Figure *34*, where the vertical axis indicates amplitude in dB and the horizontal axis shows normalized frequency range. It shows a uniformly distributed force across the all frequency range of the torquemeter. 3 dB and 10 dB drop-offs are illustrated that are respectively at 126.60 and 130.92 normalized frequency.

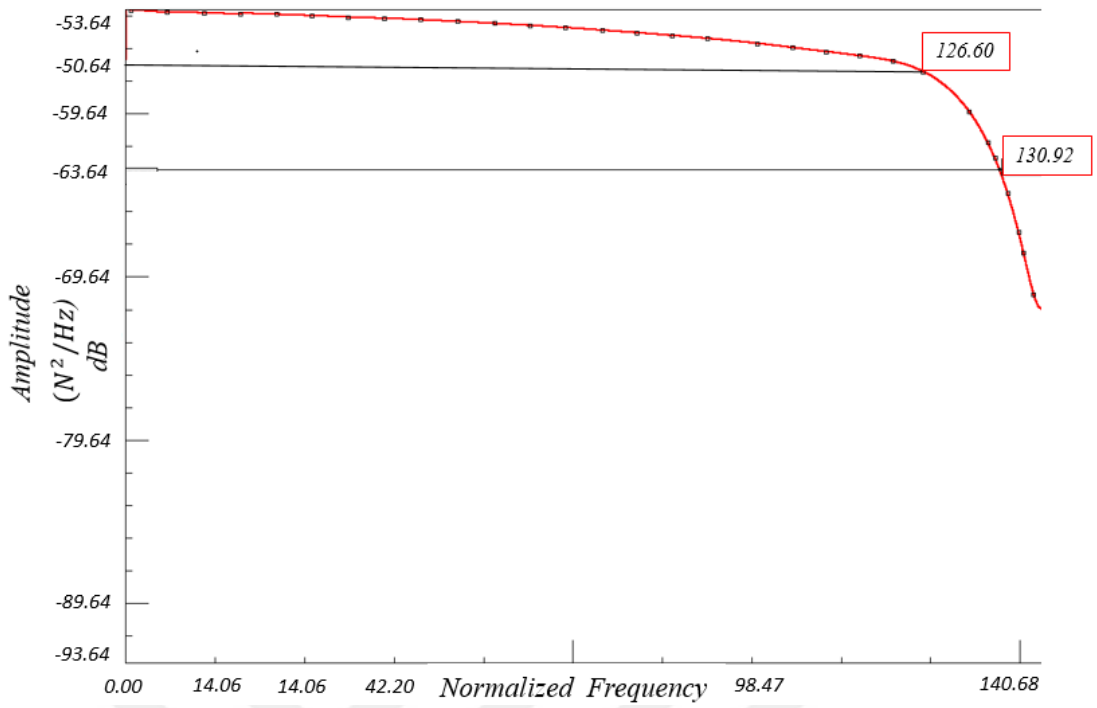

Figure 34 Input Force vs. Frequency Graph

During the test, the FRFs and corresponding coherence values shall be monitored and examined. An example of measurement FRF and its corresponding coherence function during the test is given in Figure *35* and Figure *36*. The FRF, where inputs in force (Newton) and outputs in displacement (mm) so amplitude in mm/N, show peaks that are an indicator of the presence of the natural frequencies of the Torquemeter under test. The peaks' skinny width indicates the low damping ratios for the Torquemeter as the peak width is proportional to damping. The repeatability, quality, and consistency of the individual FRF are validated by the coherence function that changes between 0 and 1. Figure *36* shows coherence values above the threshold value 0.9 at natural frequencies when the amplitude of the FRF is high. However, it indicates coherence values close to 0 at anti-resonance when the amplitude of the FRF is low. It results from the low signals because the instrumentation's noise floor is higher, which is normal and acceptable.

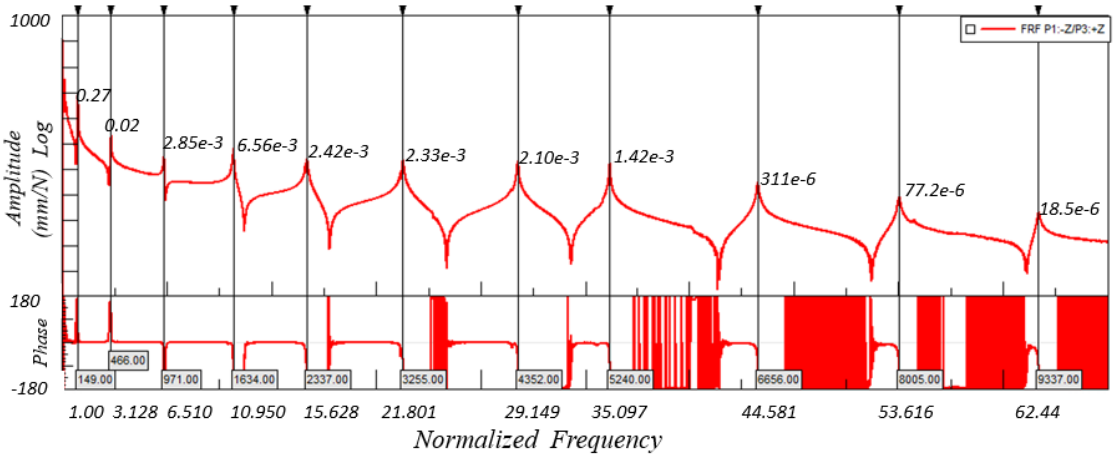

Figure 35 Amplitude and Phase of a FRF Function

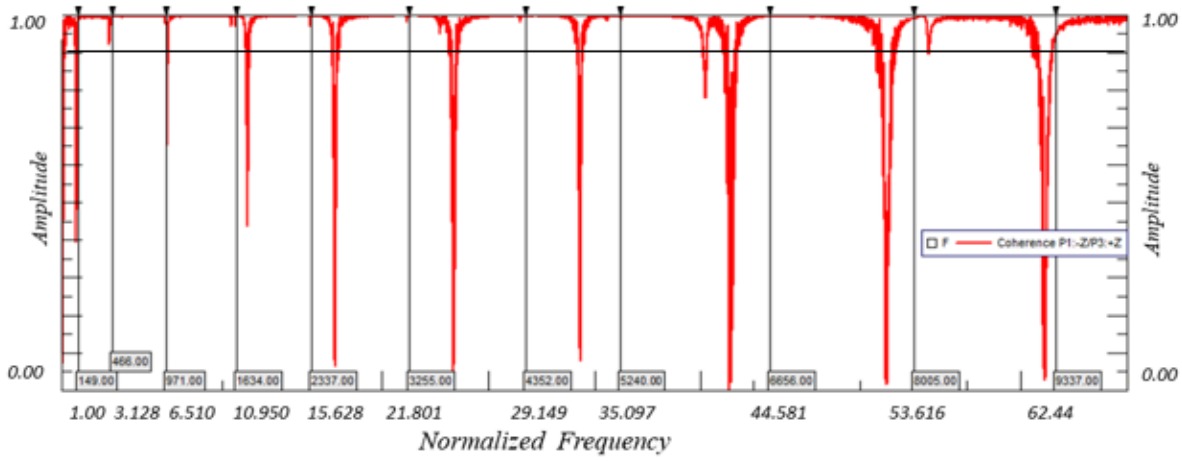

Figure 36 Coherence Function

After FRFs are measured, they are examined to extract the natural frequencies, mode shapes, and damping corresponding to each mode. LMS Test Lab17 Impact Testing Module software provides a mathematical model that makes mathematical computations for the modal curve-fitting process. The natural frequencies are extracted through curve fitting, and they are listed in Table *3*.

Table 3 Normalized Natural Frequencies of Hammer Test & Modal Analysis

Configuration	On Rubber	Hanging	Modal Analysis
Mode No.	Frequency	Frequency	Frequency
1	1.006	**1 (reference)**	1.006
2	3.123	3.128	3.099
3	6.523	6.510	6.399
4	10.965	10.950	10.833

Natural frequencies results indicate that different configurations such as hanging the torquemeter or putting on rubber do not affect the modal behavior in a general manner. The results are very close to each other, the maximum difference is almost 0.6 % at first mode, and it is not considered in terms of modal behavior. Comparing the natural frequencies with the modal analysis results shows that the free-free modal analysis's validation conforms as the maximum difference is almost 1.8 % that is the third mode, and it can be acceptable in terms of modal validation. The results indicate that the validation of the free-free modal analysis is compatible.

3.6. **Prestressed Modal Analysis Preprocessing and Solution**

The validated free-free modal analysis by the impact hammer test indicates that the meshed geometry model, with its material properties and connections, is validated through natural frequencies and mode shapes. However, the design has to be optimized by prestressed modal analysis instead of free-free one, as vibration criterion requires that there shall not be any crossing within the ± 10 % of the turboshaft engine operational speed to avoid resonance and destructive vibration by design practice.

Both free-free and prestressed modal analysis have natural frequencies for the structure but under different conditions. Prestressed modal analysis is a dynamic frequency analysis to examine the structure's vibrational behavior under predefined applied loads. For the torquemeter, these loads are defined in the static structural analysis section,

mainly caused by temperature, rotational velocity, clamp load, and an interference fit. These predefined loads and environmental conditions have an impact on the vibrational characteristics of the structure. The prestressed modal analysis includes these influences, and it provides a more realistic estimate of natural frequencies during operation.

In general, one can state that if the prestress is in tension, the natural frequencies will increase. Oppositely, if prestress is in compression, natural frequencies will decrease. For the prestressed modal analysis, static structural analysis, and validated meshed geometry model of the torquemeter with its material properties and connections are used. For the prestressed modal analysis setup, the static structural analysis solution level is linked to the modal analysis setup level. The static structural analysis result becomes an initial condition for the modal analysis.

In the analysis settings, the maximum mode to find is set to 10. Under solver controls, the damped option is enabled, and the solver type is set to full damped to enable the Coriolis Effect under rotor dynamics controls, which includes the gyroscopic effects. Rotational velocity is implemented in the x-direction as 23,000 rpm for the engine steady-state operational velocity as it is needed to compute the gyroscopic stiffness that affects the natural frequencies. In rotor dynamics controls, the Campbell diagram is enabled to identify the crossings that are a coincidence of the natural frequencies of the torquemeter with engine operational frequency.

When the solution is complete, the solution branch is displayed with a bar chart and table listing natural frequencies. The normalized natural frequencies are given in Table *4*.

Table 4 Normalized Natural Frequencies of Prestressed Modal Analysis

Mode No.	Frequency (Hz)
1	0.933
2	0.957
3	3.003
4	3.070
5	4.564
6	6.199

7	6.298
8	6.680
9	6.729
10	8.764

Mode shapes are given in Figure 37 that indicates deformation through colored counters from red (maximum) to blue (minimum), but the deformation magnitudes on the resulting legend are relative. The first bending mode consists of backward whirling Mode-1 and forward whirling Mode-2 that have normalized natural frequencies, respectively 0.933 and 0.957, which indicate forward, and backward whirlings are close to each other for the torquemeter. The maximum deformation is on the second middle ring located axially concerning the modal analysis results by excluding middle rings from the model. Similarly, the second bending mode consists of backward whirling Mode-3 and forward whirling Mode-4 that have normalized natural frequencies, respectively 3.003 and 3.070. The maximum deformation is on the first and third middle rings located axially concerning the modal analysis results by excluding middle rings from the model, which has first bending mode at 1.003 and second bending mode at 3.205. Comparing its normalized natural frequencies with prestressed modal analysis indicates that natural frequencies decrease by 5% when the middle rings are included in the model because of the middle rings' mass. However, their mode shapes are very similar.

Mode-5 is a torsional mode that has a normalized natural frequency of 4.564. The third bending mode consists of backward whirling Mode-6 and forward whirling Mode-7 that have normalized natural frequencies, respectively 6.199 and 6.298.

In a general manner, the prestressed modal analysis's bending mode shapes are similar to the free-free modal analysis results. Comparing their natural frequencies results for the same modes indicates that the difference is a maximum of 8%, so one can state that the predefined loads and environmental conditions have not much impact on the vibrational characteristics of the torquemeter.

The stiffness value is changed to 28,582 N/mm for Viton-90 using Eq. (3) to indicate the O-ring material's impact on the natural frequencies. The solution indicates that natural

frequencies increase only by 1%. Therefore, one can state that the O-ring's stiffness value does not have much impact on natural frequencies.

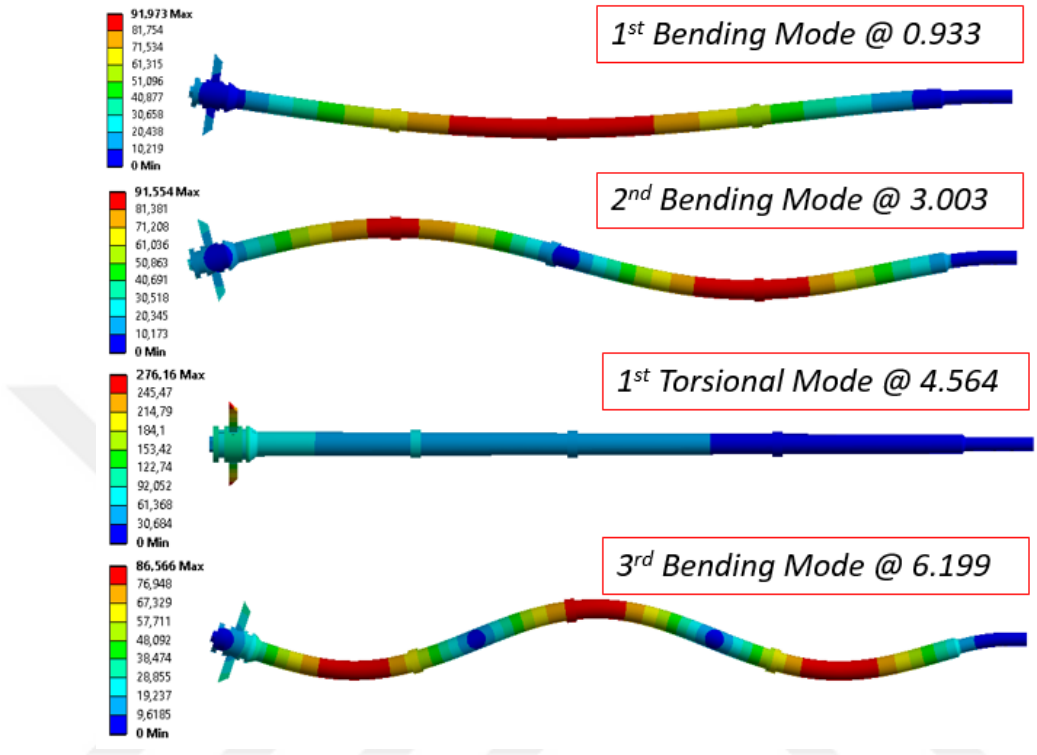

Figure 37 Mode Shapes of Prestressed Modal Analysis

The Campbell diagram assessment shall be done for crossings, which are defined as coincidences of the given natural frequencies of the torquemeter with the turboshaft operational speed range, to meet the vibration design criteria. The Campbell diagram is a practical approach to examine the modal vibrational excitation with the operating speed range because it shows the critical speed. The Campbell diagram plot is given in Figure *38* that illustrates the engine rotational speed in rpm along the x-axis and normalized frequencies along the y-axis. The inclined line is defined as the engine order line that has a ratio of one. The ratio of one means 1 rpm is equal to 1/60 Hz. The ratio of the engine order line depends on disturbing sources for vibrational characteristics. For instance, a turbine disc; the number of blades on turbine disc is considered disturbing sources. As the torquemeter carries only one blade and no other disturbing source, the engine order ratio is equal to one. Horizontal lines are natural frequencies that consist of forward and backward whirling lines because of the gyroscopic effect. As natural frequencies of

backward and forward whirling close to each other for the torquemeter, the natural frequency lines are almost overlapped.

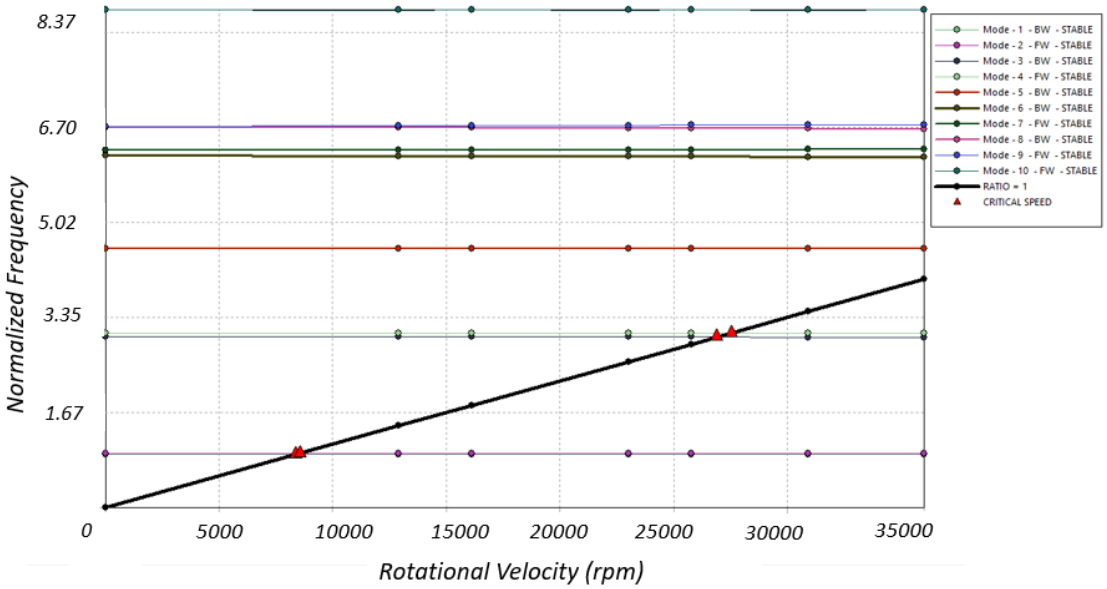

Figure 38 Campbell Diagram

There are two crossings with the first engine order line that are defined as critical speeds considering natural frequencies, and they are illustrated with the red triangles in the Campbell diagram. Four red triangles are shown in the diagram; however, two are for the same mode shapes. One is for backward whirling while the other one is for forward whirling. There shall not be any crossing between the operating below limit 20,700 rpm and its above limit 25,300 rpm because vibration design criteria require no crossing within the ± 10 % of the turboshaft engine operational speed 23,000 rpm. The first critical speed is 8601.81 rpm, a transient operating condition and below the operating speed. The second critical speed is equal to 27,700.79 rpm that is above the operating speed. Examining the Campbell diagram's critical speeds indicates that the vibration design criterion is met for the torquemeter.

4. CONCLUSION and FUTURE WORK

4.1. Conclusion

The conceptual design and analysis of the generic torquemeter under TMU for Turboshaft Engines is done with respect to design criteria. In conclusion, both strength and vibration criteria are met for the torquemeter design.

The static structural analysis results indicate that the factor of safety (FOS) is calculated as 2.20, which can be considered over design. However, the residual stresses on the torquemeter welding joints are measured via XRD. Including equivalent stresses, FOS is calculated as 1.86. As strength criterion is met, stress relievement via heat treatment on welding joints is not required, but it can be an alternative to have higher FOS. The material change would be an option for the torquemeter to reduce the cost by having FOS between 1.25 and 2.00 to be on the safe side (Dobrovolsky & Zablonsky, 1978). Inconel 718 is ductile; it has high corrosion resistance and, most importantly, keeps its strength under a wide range of operating temperatures. Therefore, it is highly demanded in the aviation industry, but it is not readily available because of its high cost.
The prestressed modal analysis results indicate the Campbell diagram, which identifies no crossing within the ± 10 % of the turboshaft engine operational speed to avoid destructive vibration. The meshed geometry model of the free-free modal analysis is validated via the impact hammer test. For further studies on vibration, the torquemeter's mechanical integrity under cyclic load can be examined. Fatigue criteria require to define the LCF and HCF service life are met. Because of very low normal stresses on the torquemeter, one can state that LCF is not concerned for the torquemeter. However, to examine the HCF service life under the Goodman diagram, the alternating stresses shall be obtained from Harmonic Analysis that shall be done after the prestressed modal analysis.

The total length (l) and the tube's wall thickness (d) can vary concerning the specified shaft geometry to use the generic conceptual design of the torquemeter for different power

output shafts. The same structural and modal analysis shall be done to check if the design criteria for strength and vibration are met.

4.2. Future Work

Reliability is vital for modern compact turboshaft engines that necessitates sufficient real-time measured data for control and diagnostics purposes. It pushes the limits to design the perfect measurement systems for turboshaft engines. TMU of modern turboshaft engines uses the angular twist method to measure the torque in a practical way for sufficient real-time measured data. Though TMU can serve as a standalone device for torque measurement, the torque data calibration precision is required as it consists of some errors. The paper elaborates on the need for a particular procedure calibration process because TMUs are not ideal, and each unit has its performance. The study aims to answer questions such as how much the worst error level is at torque measurement of the TMU, the sources of error, and if it is possible to achieve the desired accuracy with the specified calibration process (Yepifanov, Sirenko, & Zelenskyi, 2019).

The relation between the transmitted torques versus power shafts twisting angle is necessary as it is embedded in the control system to measure the torque. To find the relationship between torsional deflection of the power shaft versus transmitted torque, one may run FEA or make a hand calculation including the expected steady-state range of all the operating transmitting torques and temperature. Output shall be a diagram that indicates the twisting angle versus transmitted torque to be embedded in the algorithm. It is essential to remind that the twisting angle versus transmitted torque is derived for the universal performance of the TMU with zero allowances of manufacturing tolerances and without inaccuracies.

The method proposes that torque measurement is experimentally checked on the testbed to answer the worst error level without calibration. The TMU is integrated with the certified 'JSC Motor Sich' turboshaft engine without any calibration process then the testbed is set. The testbed was equipped with a hydraulic brake dynamometer that consumes the power of the power turbine. The testbed's control system allows setting any

torque value within the steady-state range of the tested engine. The integrated TMU measures the torque value with the embedded algorithm and the external torquemeter of the certified testbed, and it has a confidence level of 99.9 %. The temperature of the parts of the TMU and the power shaft is not measured directly because of the complexity of the measuring data from rotating parts; however, the temperature of fixed gas streamlining parts that are closed to TMU's parts are recorded.

The performance of the TMU without calibration is examined after the engine test. Figure *39* indicates the torque values in 0.001*Nm versus twisting degree*0.1 of the power shaft. The straight line is for theoretical performance, whereas the dashed line shows experimentally measured data.

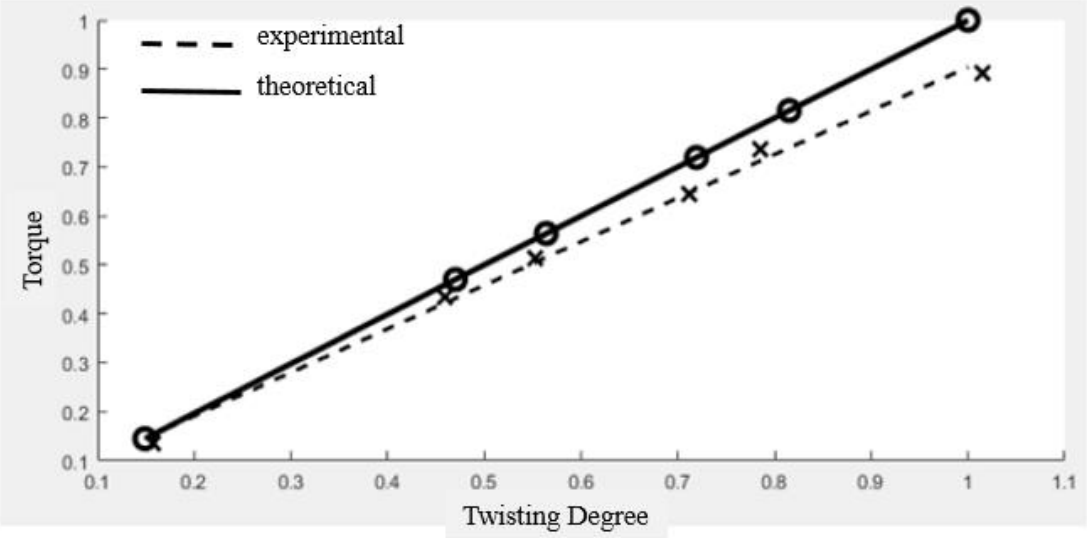

Figure 39 Experimentally Measured Data versus Theoretical Performance

The difference between the two lines refers to an error in torque measurement. The maximum total error is calculated as 11.6 % that answers the first question. This physically means that control system engineers must set the power limit to 11.6 %; in other words, 11.6% of power is paid for the safety that is not acceptable.

To answer the second question of the total error sources and decompose it into sources for estimating their impact, precision analysis is applied. Before identifying sources of the errors, first the relation between the transmitted torque (T) value and the twisting angle (α) is examined that given in Eq. (5)

$$\alpha = T\frac{L}{GI} \tag{5}$$

L is measuring the shaft's base length, the distance between the fixed pin and the center of teeth from where the twisting angle is sensed. I is for a polar moment of inertia given for the hallow power shaft in Eq. (6), where D stands for external diameter and d stands for inner diameter.

$$I = \frac{\pi}{32}(D^4 - d^4) \tag{6}$$

G is the shear modulus that is the material-dependent property, and it is changing with respect to temperature. G and I are the factors that change the resistance to torsion. Geometrical changes in the inner and outer diameters of the shaft affect the polar moment of inertia. The material properties and temperature state of the shaft affect the shear modulus. The precision analysis is done by changing these parameters, and in conclusion, the total error is decomposed into six sources: manufacturing tolerances, temperature, material properties, assembling centrifugal force, and measuring method errors.

Though the manufacturing process achieves specified tolerances, manufacturing accuracy is always limited, and the change in diameters affects the torque measurement up to 8%. Material properties can be changed from lot to lot, affecting the shear modulus, but this change is expected to be less than 1%. As shear modulus is dependent on temperature, it also changes with respect to a temperature such as 50°C error in temperature leads to 1.3 % error in torque measurement depending on the used material. Temperature also causes strains of the shaft. Circumferential strains are not considered, but 50°C error in temperature leads to axial strains causes up to 0.42 % error and radial strains cause up to 1.32 %. Assembly caused error leads up to a 2 % error in torque measurement. Centrifugal forces do not make considerable changes to the measured torque. The measuring method itself consists of 2.2 % error because of the desecrate measurements. In summary, the significant sources of the error are tolerances of external and internal shaft machining, temperature straining, material properties, and assembly.

The stages of the calibration process aim to eliminate or to minimize these significant sources of error. As each manufactured TMU integrated power shaft has its performance

and characteristics, they shall be calibrated. First, a zero-torque dynamic calibration is conducted to get the teeth' exact initial relative position to eliminate the assembly error. Then the exact internal and external diameters of the manufactured power shaft are measured. FEA is rerun with these exact dimensions and former temperature data from engine tests; output is the twisting angle versus transmitted torque. Then the residual is calculated by subtracting the calculated twisting angles from the expected ones. The adjustment is implemented in the engine automatic control system's control algorithm to eliminate the calculated residual. After that, the certified engine rig test is repeated to answer the third question if it is possible to achieve the desired accuracy with the specified calibration process. The results show that the individual calibration process sustains considerable profit in the torque measurement accuracy. Figure *40* indicates the torque values in 0.001*Nm versus twisting degree*0.1 of the power shaft, so the torque measurement error of the calibrated TMU integrated power shaft is less than 1 % (Yepifanov, Sirenko, & Zelenskyi, 2019).

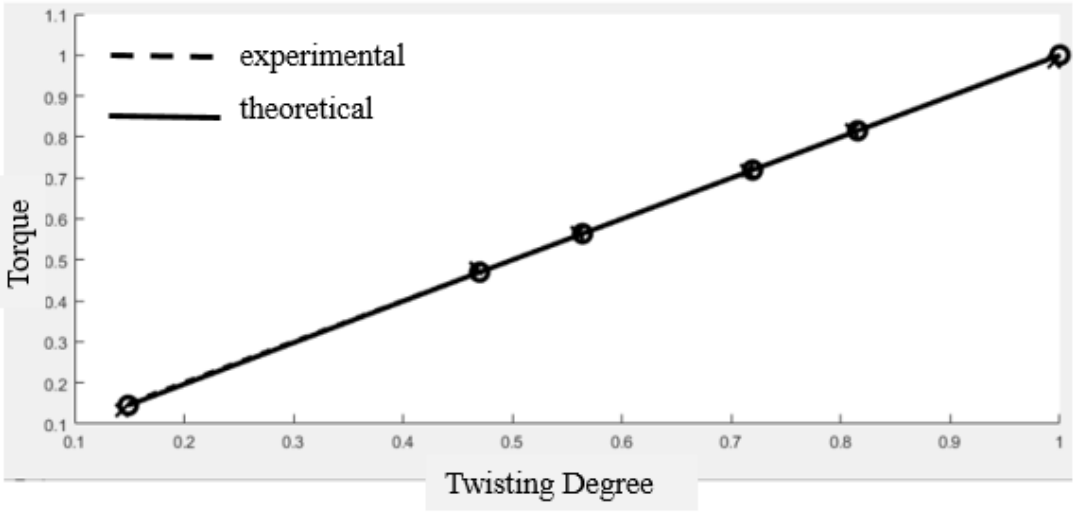

Figure 40 Experimentally Measured Data versus Theoretical Performance-2

This study has highlighted the necessity of the developed calibration process for the TMU that uses the phase angle difference method in future work. Each TMU integrated power shaft requires to be calibrated individually for the acceptable confidence level of torque measurement. Engine rig test shall be applied to verify the calibration processes by comparing the values of the TMU and directly measured by the external torque measuring system.

5. BIBLIOGRAPHY

Acker, B. N. (2006). *United States Patent No. 7051535.*

AGARD. (1994). *Advisory Group For Aerospace Research& Development, Guide to the Measurements of the Transient Performance of Aircraft Turbine Engines.* Ottawa: AGARD, Nort Atlantic Treaty Organization.

Aranson, M., & Nelson, R. (1964). *Torque Handbook.* Instruments Publishing Co.

Aviation, G. (2020, 03 02). *GE Aviation Military Engines*. Retrieved from GE Aviation Military Engines- T700 Engine: https://www.geaviation.com/military/engines/t700-engine

Becker, M. D., & Frounfelker, B. (1992). Gyroscopic Test for the T800-LHT-800. *SAE Technical Papers Series*.

Bodin, R. M. (2013). *US Patent No. US8549931.*

Center, G. R. (2015, 05 05). *NASA Torque*. Retrieved from National Aeronautics and Space Administration Web Site: https://www.grc.nasa.gov/www/k-12/airplane/torque.html

Chang, D. J., & Kukel, D. J. (1973). *Advanced Torque Measurement System.* Virginia: Ai Research Manufacturing Company, U.S. Army Air Mobility Research and Development Laboratory.

Dobrovolsky, V., & Zablonsky, K. (1978). *Machine Elements.* Moscow: Peace Publisher.

Doebelin, E. O. (1966). *Measurement Systems: Application and Design.* The Ohio State University: McGraw-Hill Inc.

Douglas, L. (1991). Development of a Lubrication System for the T800 Turboshaft Engine. *ASME*.

EASA. (2008, August 4). *European Aviation Safety Agency.* Retrieved from European Aviation Safety Agency: https://www.easa.europa.eu/sites/default/files/dfu/EASA-TCDS-E.232_(IM)_Light_Helicopter_Turbine_Engine_Company_(LHTEC)_series_engines-01-04082008.pdf

Engines, S. H. (2020, 02 03). *Safran Helicopter Engines*. Retrieved from Safran Helicopter Engines: https://www.safran-helicopter-engines.com/helicopter-engines/over-2000-shp/rtm322

Fuller, D. D. (1940). *Coefficients of Friction, Columbia University.* Retrieved from MIT EDU: https://web.mit.edu/8.13/8.13c/references-fall/aip/aip-handbook-section2d.pdf

Howard, D. W., & Wintrode, W. C. (1963). *United States Patent No. 3114240.*

Howard, D. W., & Wintrode, W. C. (1963). *US Patent No. 3114240.*

Hünecke, K. (1997). *Jet Engines: Fundamentals of Theory, Design, and Operation.* Osceola: Motorbooks International.

Kandil, F. A., Lord, J. D., & T., F. A. (2001). *A Review of Residual Stress Measurement Methods.* Middlesex: HMSO.

Lewis, D., & Buller, M. J. (1985). The Conception and Development of a Family of Small Engines for the 1990s. *AIAA/SAE/ASME 21st Joint Propulsion Conference* (p. 8). Monterey: AIAA.

MatWeb. (2011). Retrieved from MatWeb, Material Property Data: http://www.matweb.com/services/services.aspx

Morinaga, M. (2018). *A Quantum Approach to Alloy Design.* Elsevier.

NASA. (1977). *Stiffness and Damping of Elastomeric O-ring Bearing Mounts.* National Aeronautics and Space Administration, Lewis Research Center.

NASA, G. R. (2015, 05 05). *NASA Torque*. Retrieved from National Aeronautics and Space Administration Web Site: https://www.grc.nasa.gov/www/k-12/airplane/torque.html

Raymond, S., & Baker, D. (2010). *United States Patent No. 7698959.*

Raymond, S., & Baker, D. (2010). *US Patent No. 7698959.*

Rolls-Royce. (1996). *The Jet Engine.* Birmingham: Renault Printing Co. Ltd.

Scoppe, F. E. (1973). *Advanced Torque Measurement System Technique.* Stratford: Avco Lycoming Division, U.S. Army Air Mobility Research and Development Laboratory.

Siemens. (2019, August 29). *Modal Tips: Roving Hammer versus Roving Accelerometer.* Retrieved from Siemens Community Article: https://community.sw.siemens.com/s/article/modal-tips-roving-hammer-versus-roving-accelerometer#:~:text=Roving%20the%20impact%20hammer%20has,could%20alter%20the%20natural%20frequencies.

Siemens. (2020, July 10). *What is the Frequency Response Function (FRF).* Retrieved from What is Frequency Response Function (FRF): https://community.sw.siemens.com/s/article/what-is-a-frequency-response-function-frf

Sirenko, F., Yepifanov, S., Podgorsky, K., & Nechunaev, S. (2018). New Approach to Torque Measurement Unit Development and its Calibration. *Journal of Konbin*, 12.

Stresstech. (2020). *X-ray Diffraction.* Retrieved from Stresstech XRD: https://www.stresstech.com/knowledge/non-destructive-testing-methods/x-ray-diffraction/

Suominen, L., Khurshid, M., & Parantainen, J. (2013). Residual Stress in Welded Components Following Post-weld Treatment Methods. *Procedia Engineering*, 181-191. Retrieved from Stresstech: https://www.stresstech.com/stresstech-bulletin-15-residual-stress-in-welding/

Trelleborg O-Ring Calculator, T. S. (2020). *Trelleborg O-Ring Calculator*. Retrieved from Trelleborg O-Ring Calculator: https://www.tss.trelleborg.com/en/resources/design-support-and-engineering-tools/o-ring-calculator

US Army Aviation, W. C. (2007, DECEMBER). T700 ENGINE STUDENT HANDOUT. FORT RUCKER, ALABAMA, USA.

Yepifanov, S., Sirenko, F., & Zelenskyi, R. (2019). The Precision Analysis of a Relative Phase Difference Torque Measurement Unit. *AERO-UA, Horizon 2020 Programme, Strategic and Targeted Support for Europe Ukraine Collaboration in Aviation Research.* Ukraine: NATO OTAN.